Precambrian Research 439 (2026) 108107

Contents lists available at ScienceDirect

Precambrian Research

journal homepage: www.elsevier.com/locate/precamres

Sedimentology, petrography, and carbon isotopes of the ~ 2.2 Ga Kona Dolomite, Upper Peninsula of Michigan

Maya L. Giannecchini [a,*], Garrett D. Brown [b,c], Cory M. Redman [d], Ian Z. Winkelstern [a], Dylan T. Wilmeth [a]

[a] Department of Geology, Grand Valley State University, Grand Rapids, MI 49401, United States
[b] Department of Plant Biology, Michigan State University, East Lansing, MI 48824, United States
[c] Department of Biology, Grand Valley State University, Grand Rapids, MI 49401, United States
[d] Grand Rapids Public Museum, Grand Rapids, MI 49504, United States

ARTICLE INFO

Keywords:
Geobiology
Geochemistry
Stratigraphy
Stromatolites
Sedimentology

ABSTRACT

The Lomagund-Jatuli Event (LJE), was the largest and most prolonged positive $\delta^{13}C$ excursion in Earth's history (2.3–2.0 Ga). Many LJE carbonates have $\delta^{13}C$ values above + 5‰ VPDB. The origins of these enriched values is still debated between the influences of global carbon burial vs. local environments such as restricted, evaporitic basins. The Kona Dolomite in the Upper Peninsula of Michigan, USA, is an exposed LJE-era carbonate in the Lake Superior region. The Kona Dolomite is exposed in western and eastern Marquette, Michigan. The western Kona Dolomite contains gypsum pseudomorphs, microbial roll-up structures and persistent stratiform stromatolites, indicating a peritidal, evaporative sabkha environment. In eastern exposures, giant domal stromatolites indicate a lateral transition to deeper intertidal and subtidal environments. Despite facies differences, new $\delta^{13}C$ values of western Kona deposits closely resemble previous measurements from eastern deposits, both exceeding + 8‰. While textural evidence indicates secondary alteration, there is no correlation between $\delta^{13}C$ and diagenetic proxies such as $\delta^{18}O$ and Mn/Sr. The apparent lack of difference in $\delta^{13}C$ between western and eastern Kona facies could be due to relative proximity despite different facies, or post-depositional alteration, or the relative lack of correlation between eastern and western Marquette. A facies-dependent trend is observed when comparing $\delta^{13}C$-enriched, evaporitic carbonates such as the Kona with $\delta^{13}C$-"depleted" subtidal formations in the region.

1. Introduction

The Paleoproterozoic Era (2.5–1.6 Ga) was marked by major changes in global chemistry and biology including the Lomagundi-Jatuli Excursion (LJE), the longest positive carbon isotope excursion in Earth history (~2.3–2.0 Ga). The LJE contains some of the most positive $\delta^{13}C$ values recorded in marine carbonate rocks (+5 to + 30‰), compared with typical values of ~ 0‰ in ancient and modern carbonates (Martin et al., 2013; Prave et al., 2022; Hodgskiss et al., 2023). The mechanisms behind the LJE are still widely debated, with several different models proposed. The canonical LJE model starts with the Great Oxidation Event (GOE) increasing atmospheric O_2 from microbial activity (Karhu & Holland 1996; Melezhik et al., 1999). A rise in atmospheric oxygen in the atmosphere may have accelerated weathering, supplying the oceans with more nutrients such as phosphorus (Bekker & Holland 2012). The growth of continental crust may also have provided larger surface areas to weather, increasing the nutrient flux and potentially boosting primary productivity, driving organic carbon burial and depositing organic carbon concentrated in ^{12}C (Bindeman 2021). As more organic carbon was buried, $\delta^{13}C$ values of marine dissolved inorganic carbon (DIC) would become more positive, as reflected in inorganic carbonate deposits. The GOE, LJE, and continental growth all occurred between 2.5 and 2.0 Ga, but the exact relationships between these events remain unclear after a half-century of study (Hodgskiss et al., 2023).

An alternative facies-dependent model has also been proposed to explain $\delta^{13}C$ patterns during the LJE. Surveys of many LJE-era carbonates reveal that deeper and more open-marine sedimentary facies record smaller $\delta^{13}C$ shifts (+1.5‰) than shallow, evaporative facies (+8‰) (Prave et al., 2022; Hodgskiss et al., 2023). In modern shallow marine environments, enriched $\delta^{13}C$ values are due to enhanced primary productivity, which can be amplified in restricted, evaporative embayments (Aharon et al., 1977; Schidlowski et al., 1985; Swart et al., 2009;

* Corresponding author.
E-mail address: giannecm@mail.gvsu.edu (M.L. Giannecchini).

https://doi.org/10.1016/j.precamres.2026.108107
Received 4 August 2025; Received in revised form 2 April 2026; Accepted 7 April 2026
Available online 15 April 2026

Geyman & Maloof, 2019; Chen et al., 2022; Trower et al., 2024). The loss of ^{12}C through evaporation and degassing in such environments has also been proposed to elevate $\delta^{13}C$ (Melezhik et al., 1999; Prave et al., 2022). The canonical and facies-dependent models are not mutually exclusive, as expanding shallow continental shelves would likely have increasing amounts of restricted, evaporitic shallow environments, and high rates of organic carbon production and burial. Differentiating global vs. local influences on LJE chemistry requires investigating the depositional environments that create conditions ideal for $\delta^{13}C$ enrichment.

Several Paleoproterozoic deposits in the Lake Superior region contain LJE-era carbonates (Fig. 1) with widely varying isotopic compositions (Bekker et al., 2006). Of these deposits, only two contain $\delta^{13}C$-enriched carbonates (>+5‰): the 2.17 Ga Kona Dolomite in Michigan's Upper Peninsula, and the 2.31 Ga Gordon Lake Formation on the northern shore of Lake Huron, Ontario (Bekker et al., 2006). Many previous Kona Dolomite studies have focused on eastern Marquette, near the Lake Superior shoreline (Twenhofel, 1919; Gair & Thaden 1968; Nordeng, 1963; Taylor, 1972; Wohlabaugh and Mancuso, 1990; Bekker et al. 2006; Ramsay et al., 2025). In contrast, the western two-thirds of Kona exposure are relatively understudied in recent years (van Hise & Bayley, 1895; Taylor, 1972; Gair, 1975; Wohlabaugh, 1980; Ramsay et al., 2025). Despite over a century of study, only one published article is specifically dedicated to Kona stratigraphy, which only focuses on one member of the Kona Dolomite, the Big Cusp algal dolomite unit (Wohlabaugh and Mancuso, 1990).

The Lindberg Quarry in western Marquette has excellent, extensive exposures of the Kona Dolomite, many which remain undescribed, providing a unique opportunity to further understand Kona environments during the LJE. This study expands the current knowledge of the Kona Dolomite by providing detailed stratigraphy and petrography of sedimentary features, and stromatolites around Lindberg Quarry. The stromatolites and surrounding sediment layers are used to interpret environmental changes over time, including wave energy and relative water depth. This study also adds new isotope and elemental data as $\delta^{13}C$, $\delta^{18}O$, and Mn and Sr ratios, enabling new insights into both original depositional environment and diagenesis.

2. Geologic setting

2.1. Regional stratigraphy

The Kona Dolomite is part of the larger Marquette Range Supergroup, which is exposed throughout Michigan's Upper Peninsula and northern Wisconsin (Fig. 1; Cannon & Gair, 1970). The Marquette Range Supergroup is divided into three stages: the Chocolay, Menominee, and Baraga Groups (Cannon & Gair, 1970). Sediment deposition started during the Chocolay Group (2.2–2.3 Ga) as sandstones and dolomites onto older Archean Superior Craton basement. As the Archean basement rifted apart, volcanic rocks, shales and iron formations of the Menominee Group (1.9 Ga) were deposited in expanding basins. The Baraga Group (1.86–1.85 Ga) are deep-water deposits that formed as island arcs collided with previous shorelines.

Around Marquette, Michigan, the Chocolay Group contains four

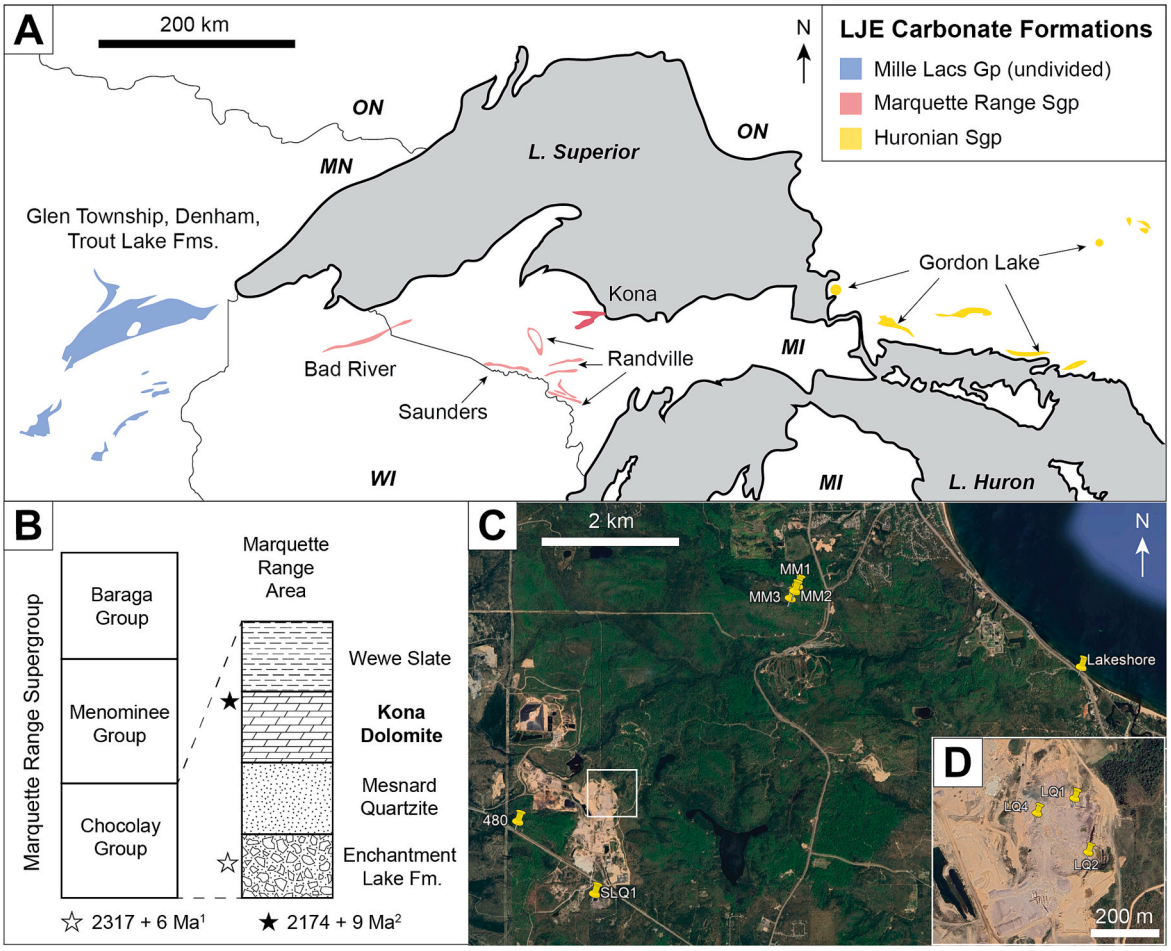

Fig. 1. A) LJE-era carbonates around the Lake Superior region. B) Stratigraphy of the Marquette Range Supergroup. Age references: 1: Vallini et al., 2006; Rasmussen et al., 2024. C) Aerial map of visited localities of the Kona Dolomite (Pins). LQ = Lindberg Quarry, SLQ= South Lindberg Quarry, 480= Highway 480, MM = Mount Mesnard.

units (Pettijohn, 1943). The Chocolay Group starts with conglomerates of the Enchantment Lake Formation, followed by coastal beach deposits of the Mesnard Quartzite, then shallow-water environments of the Kona Dolomite, concluding with the Wewe Slate, representing rising sea levels over time.The Kona Dolomite is up to 800 m thick covering ~ 50 km^2 (Twenhofel, 1919; Nordeng, 1963; Taylor, 1972; Wohlabaugh and Mancuso, 1990; Ramsay et al., 2025), with a maximum age constraint is 2317 ± 6 Ma, from detrital zircons in the underlying Enchantment Lake Formation (Vallini et al., 2006).. The Kona Dolomite was previously correlated with the > 2.2 Ga Gordon Lake Formation in Ontario based on similar enriched $\delta^{13}C$ signatures above + 5‰ (Bekker et al., 2006). However, Rasmussen et al., 2024 provide a new minimum Kona constraint of 2174 ± 9 Ma from basal tuffs in the conformable, immediately overlying Wewe Slate. The proximity of recently-described tuffs to uppermost Kona beds (Rasmussen et al., 2024) strongly suggests an age closer to 2174 than 2317 Ma.

The Kona Dolomite sits in an east–west syncline, with the hinge point to the east, close to the Lake Superior shore (Fig. 2), and north and south limb exposure. The oldest members are on the fringes of the syncline, younging towards the center. The north limb dips steeply to the south and has best exposure in the eastern Mount Mesnard area. The south limb dips more gently towards the north, and has more exposure (Fig. 2). Despite folding, the Kona Dolomite entirely lies within the least metamorphosed "chlorite zone" of James (1955) based on metamorphic mineral assemblages interpreted as lower greenschist-facies (300-400 °C, 2–8 kbar).

2.2. Previous Kona sedimentology

The Kona Dolomite was first described by van Hise & Bayley (1895), in a regional report for the United States Geological Survey (USGS). Subsequent USGS reports described Kona features across the entire syncline (van Hise & Bayley, 1897; van Hise et al., 1911; Gair et al., 1961), then on eastern (Gair & Thaden 1968) and western exposures (Puffett 1974; Gair, 1975). At the same time, stromatolite-focused studies described a notable locality with giant, multi-meter domes and columns, found near the lakeshore in the syncline's southern limb (Twenhofel 1919; Nordeng 1963). Subsequent USGS reports discovered abundant domal and stratiform stromatolites throughout the entire Kona region (Gair & Thaden 1968; Puffett 1974; Gair, 1975). Despite extensive documentation, the depositional interpretations of these Kona studies only described shallow marine settings, with no discussion of tidal zones or relative restriction.

The first and most detailed study of Kona sedimentology was Taylor (1972), an unpublished doctoral thesis. Taylor mapped and divided the Kona Dolomite into 11 members, using Mount Mesnard on the north limb as a type locality (Fig. 2). Taylor's lower five members are mostly fine-grained clastic argillites, with moderate quartzite and minor dolostone layers. The upper six members are dominated by dolomite, with increasing amounts of argillite over time. Taylor's 11 members have been used as a framework for subsequent studies (Wohlabaugh 1980; Wohlabaugh & Mancuso, 1990; Bekker et al., 2006; Ramsay et al., 2025), and some members have been correlated across the entire region. For example, Wohlabaugh 1980 and Wohlabaugh & Mancuso 1990 compared Taylor's Member 6 ("Big Cusp Dolomite") across the north and south limbs, including the giant lakeshore stromatolite locality. However, Taylor's 11 members remain informal, and no subsequent attempts have been made to verify correlations between the north and south limbs.

3. Material and methods

The study localities are isolated (Fig. 2), separated by faults and extensive cover. We tentatively follow Taylor's nomenclature for stratigraphic units, but specific correlations or age relationships between many individual columns cannot be made with confidence. Table 1 lists locations of stratigraphic columns and samples, while Table 2 lists sample lithology and chemistry.

The majority of samples come from western Marquette (Figs. 1 and 2), with excellent exposures from Lindberg Quarry and nearby roadcuts.

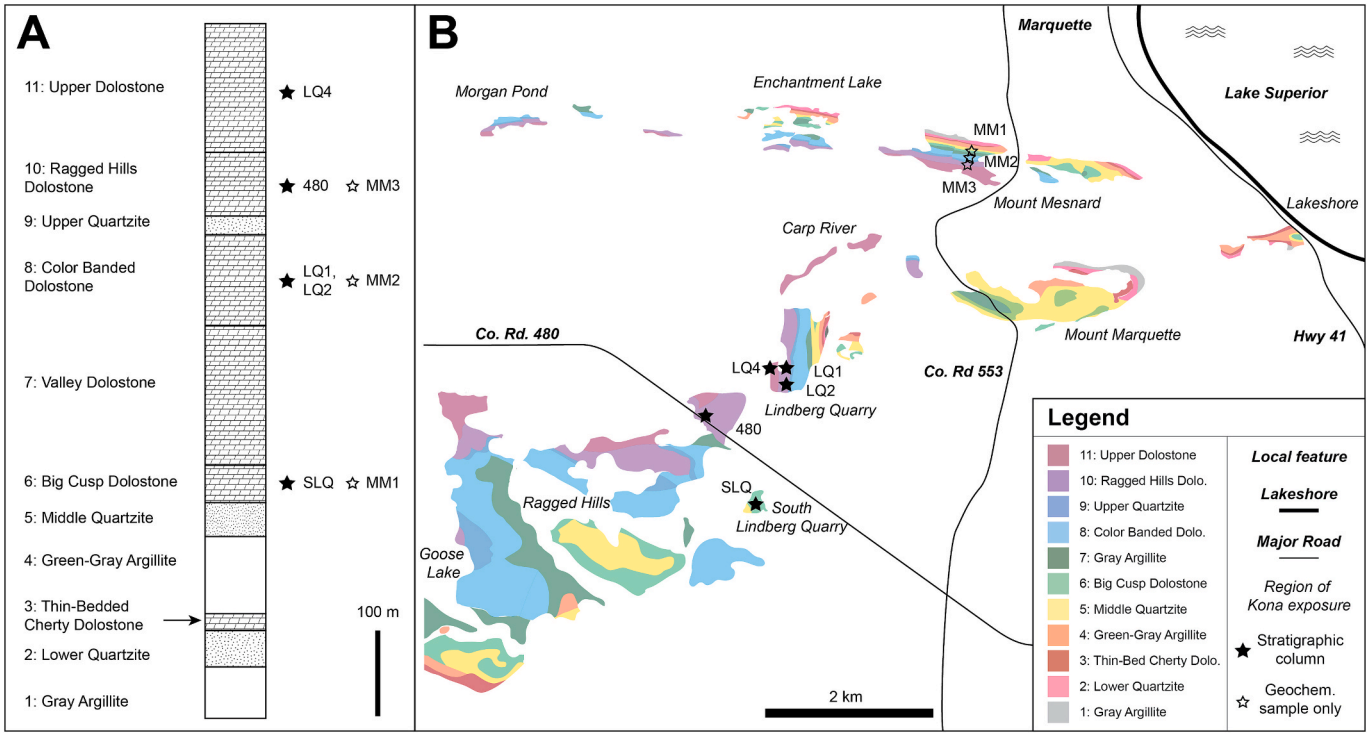

Fig. 2. The Kona Dolomite syncline and stratigraphy. A) Stratigraphic column of the Kona Dolomite split into Taylor 1972's 11 informal members with stars representing localites visited. B) Color-coded map of the Kona Dolomite syncline, modified from Taylor 1972.

Table 1
Localities of stratigraphic localities.

	Locality	Informal Member (Taylor 1972)	Coordinates	Hand Sample
W. Kona	**SLQ**	**6 "Big Cusp"**	N 46° 28.5162′ W 87° 27.5083′	SLQ-1–1
	LQ1	**8 "Color Banded"**	N 46° 29.3538′ W 87° 27.3092′	LQ1-2
	LQ2	**8 "Color Banded"**	N 46° 29.2762′ W 87° 27.2802′	LQ2-1
	480	**10 "Ragged Hills"**	N 46° 29.0888′ W 87° 28.3765′	480–1-1
	LQ4	**11 "Upper Dolomite"**	N 46° 29.3336′ W 87° 27.3880′	LQ4
E. Kona	**MM1**	**6 "Big Cusp"**	N 46° 30.9488′ W 87° 25.1855′	MM1
	MM2	**8 "Color Banded"**	N 46° 30.9046′ W 87° 25.2192′	MM2
	MM3	**10 "Ragged Hills"**	N 46° 30.8485′ W 87° 25.2683′	MM3

Table 2
All isotopic and elemental data of the Kona Dolomite from this study.

Sample	Locality	Lithology	$\delta^{13}C$ (‰)	$\delta^{18}O$ (‰)	Mn (ppm)	Sr (ppm)	Mn/Sr
1	SLQ-1–1	Stratiform strom.	5.25	−8.61	1684.2	46.1	37
2	SLQ-1–1	Stratiform strom.	5.25	−7.42	2389.7	44.1	54
3	SLQ-1–1	Stratiform strom.	4.89	−10.43	1492.2	39.1	38
4	SLQ-1–1	Stratiform strom.	5.4	−8.25	2102	47.6	44
5	SLQ-1–1	Stratiform strom.	8.05	−7.75	1888.5	70.9	27
6	SLQ-1–1	Stratiform strom.	7.64	−8.4	1222	54.5	22
7	SLQ-1–1	Stratiform strom.	7.64	−9.7	890.9	52.4	17
8	SLQ-1–1	Stratiform strom.	8.36	−6.68	1230.9	65.5	19
9	SLQ-1–1	Stratiform strom.	7.88	−8.07	857.2	37	23
10	LQ1-2	Domal strom.	7.45	−13.41	557.1	214.3	3
11	LQ1-2	Domal strom.	7.46	−13.25	517.6	223.5	2
12	LQ1-2	Domal strom.	7.33	−13.37	506.8	212.3	2
13	LQ1-2	Domal strom.	7.33	−13.64	562.9	211.9	3
14	LQ1-2	Domal strom.	7.41	−13.39	468.4	215.2	2
15	LQ2-1	Planar dolomite	6.65	−10.5	532.6	125	4
16	LQ2-1	Planar dolomite	6.26	−11.09	617.8	101.9	6
17	LQ2-1	Planar dolomite	5.37	−11.98	663.5	67.3	10
18	LQ2-1	Planar dolomite	6.86	−9.83	470.1	128.2	4
19	480–1-1	Planar dolomite	5.82	−11.34	430.5	161.4	3
20	480–1-1	Planar dolomite	5.89	−11.4	392.6	116.6	3
21	480–1-1	Planar dolomite	5.8	−11.35	428.6	115.6	4
22	480–1-1	Planar dolomite	5.96	−11.31	405.9	123.8	3
23	LQ4	Stratiform strom.	6.31	−11.59	884.6	93.4	9
24	LQ4	Stratiform strom.	6.2	−11.48	854.2	78.1	11
31	LQ4	Stratiform strom.	6.48	−10.76	1031.6	89.5	12
32	LQ4	Stratiform strom.	6.25	−11.44	822.4	79.4	10
33	LQ4	Stratiform strom.	6.37	−11.41	911.1	84.4	11
34	MM1	Domal strom	7.14	−9.25	1278.1	39.7	32
35	MM1	Domal strom.	7.23	−9.86	1029.4	36.8	28
36	MM1	Domal strom.	7.86	−8.67	1076.4	44.6	24
37	MM1	Domal strom.	7.93	−7.29	829.9	61.2	14
38	MM1	Domal strom.	3.78	−12.84	1924.6	65.3	29
39	MM1	Domal strom.	5.31	−12.47	1358	57.6	24
40	MM1	Domal strom.	4.75	−12.49	1551.9	49.2	32
41	MM1	Domal strom.	4.66	−12.94	965.2	60.9	16
42	MM1	Domal strom.	6.84	−10.18	1327.1	56.1	24
43	MM2	Planar dolomite	5.45	−12.3	1919.5	47	41
44	MM2	Planar dolomite	5.29	−12.1	1940.7	50.8	38
45	MM2	Planar dolomite	4.95	−13.21	1777	36	49
46	MM2	Planar dolomite	5.49	−12.09	1752.5	39.6	44
47	MM2	Planar dolomite	5.07	−11.77	1811.8	65.3	28
48	MM2	Planar dolomite	5.47	−12.91	1991.5	38.3	52
49	MM2	Planar dolomite	6.04	−12.16	2145.3	41.1	52
50	MM2	Planar dolomite	6.19	−11.17	1936	40	48
51	MM2	Planar dolomite	4.87	−12.29	2302	45.2	51
52	MM3	Domal strom.	7.54	−13.69	217	292.5	1
53	MM3	Domal strom.	7.49	−13.44	219	292	1
54	MM3	Domal strom.	7.59	−13.96	367	321.1	1
55	MM3	Domal strom.	7.53	−12.51	274.1	370.4	1
56	MM3	Domal strom.	5.99	−11.04	263.2	360.9	1
57	MM3	Domal strom.	6.05	−10.97	263.2	348.7	1
58	MM3	Domal strom.	5.77	−11.36	308.8	389.7	1
59	MM3	Domal strom.	6.06	−10.92	237.7	319.7	1
60	MM3	Domal strom.	6.04	−10.69	252.9	356.3	1

Locality SLQ was designated Member 6 by Taylor 1972, with subsequent stratigraphy from Wohlabaugh 1980 and Wohlabaugh & Mancuso 1990. Three stratigraphic columns were measured in the larger, active Lindberg Quarry: LQ1 and LQ2 from the quarry's east side (Member 8) and LQ4 from west side (Member 11). Locality 480 is a roadcut on Highway 480, 1.5 km northwest of Lindberg Quarry, interpreted as Member 10 from Taylor 1972. Kona Dolomite hand samples and associated isotope analyses were also collected from Mount Mesnard. Samples MM1, MM2,

and MM3 are tentatively assigned to members 6, 8 and 10 respectively from Taylor 1972. The type locality of Mount Mesnard has become densely obscured by vegetation, which also obscures potential offsets or lateral facies variations across the syncline. For example, this study was able to collect hand samples from Mount Mesnard, but did not measure stratigraphic columns. In contrast, quarrying in western Marquette has exposed abundant outcrops, including many that were unavailable during Taylor 1972's studies. As a result, this study uses the Taylor 1972 divisions as a broad guide for relative ages between stratigraphic columns (Fig. 3), but does not attempt to make strict stratigraphic correlations.

Hand samples were cut using water-cooled saws to select areas for thin-section analysis. Petrography was analyzed using an Olympus BX-51 microscope with a Jenoptik camera with mosaic software to combine multiple photographs into larger images. Hand samples were drilled for powder using a Dremel diamond burr, avoiding any fractured and recrystallized areas. A total of 50 powders were drilled from Kona Dolomite hand samples. Thirty-three powders came from Lindberg Quarry (LQ, three hand samples) and adjacent western localities (SLQ, 480, one hand sample from each locality). Seventeen powders were also drilled from three Mount Mesnard hand samples for comparison. Powdered drill samples (~0.001 g) were analyzed for $\delta^{13}C$ and $\delta^{18}O$ at the University of Michigan Stable Isotope Lab on a ThermoFisher MAT253 mass spectrometer with a Kiel IV automated preparation device. Analytical precision was better than 0.2‰ VPDB based on repeated analysis of the NBS-19 standard. Delta values were calculated using the following equation: $\delta = ((R_{sample}/R_{standard}) - 1)$ x 1000, where R is the ratio of isotopes ($^{13}C/^{12}C$ or $^{18}O/^{16}O$). Ratios of Mn/Sr were determined using 0.01 g powder from the same drill locations as isotopic measurements. A calibration curve was made from a 10 mL solution of 2% nitric acid using diluted Mn and Sr standards ($r^2 = 0.99$), following previous techniques applied to the Kona Dolomite (Bekker et al., 2006). The diluted samples were placed in an Agilent 5800 ICP-OES with a Varian SpectrAA 200 Atomic Absorption Spectrometer.

4. Results

4.1. Stratigraphy and sedimentary facies

Since not all 11 of Taylor's 1972 units were observed in this study, this study broadly divides the Kona Dolomite into three facies for the purpose of describing sedimentology and stratigraphy: stromatolitic, layered, and structureless (Fig. 3). Locations from western Marquette (Lindberg Quarry, Highway 480) are shown in Figs. 4-7, while locations from eastern Marquette (Mount Mesnard) are shown in Fig. 8.

4.1.1. Stromatolites

Stromatolites are preserved in all localities and most sedimentary facies described in this study. Stromatolite facies and morphology at each locality are described using classification and terminology from the Handbook for the Study and Description of Microbialites by Grey and Awarmik, 2020.

4.1.1.1. Stratiform. Stratiform stromatolites are found across the Kona Dolomite, in LQ, SLQ, and MM (Figs. 4, 5, 8, Supp. Fig. S1). Stratiform stromatolites at LQ had a tightly crinkled texture, with millimeter-scale laminations (Fig. 4). Stratiform layers are laterally continuous and vertically, the stratiform layers in the rock faces are pervasive, with internal microbial lamina of poor inheritance and relief observed over one meter of stratigraphy. Stratiform stromatolites often transition into other stromatolite morphologies and sedimentary features. For example, stratiform structures in LQ1 gradually change into domes 40 cm wide with 10 cm relief (Fig. 5c). A two centimeter stratiform bed at SLQ3 overlies dolostone ripple marks, inheriting the base shape (Fig. 4C). Within the stromatolite, there are millimeter scale fine crinkled textures that are not observed in the underlying ripples. Stratiform stromatolites are also found in the Mount Mesnard outcrops, but have a more undulatory, less horizontal texture, and are found in alternating layers of resistant chert and dolostone (Fig. 8a).

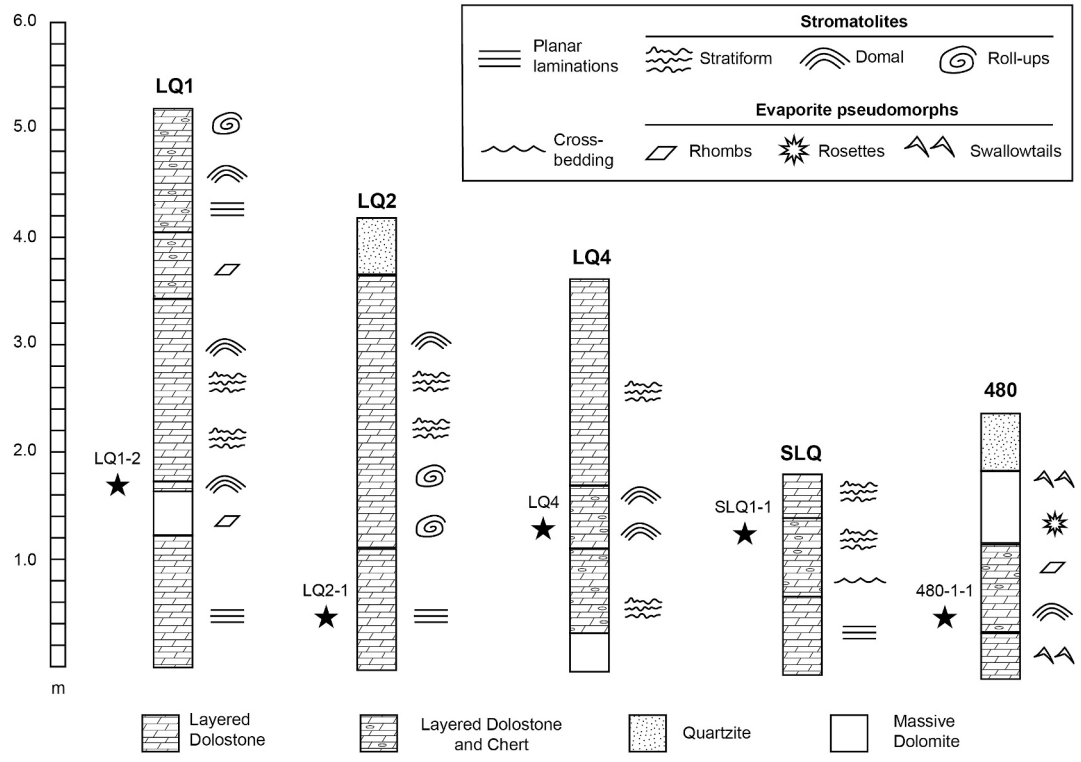

Fig. 3. Stratigraphic columns of Kona Dolomite, with key features shown for each section. Stars represent where each hand samples were collected within the stratigraphic column at every western Marquette locality.

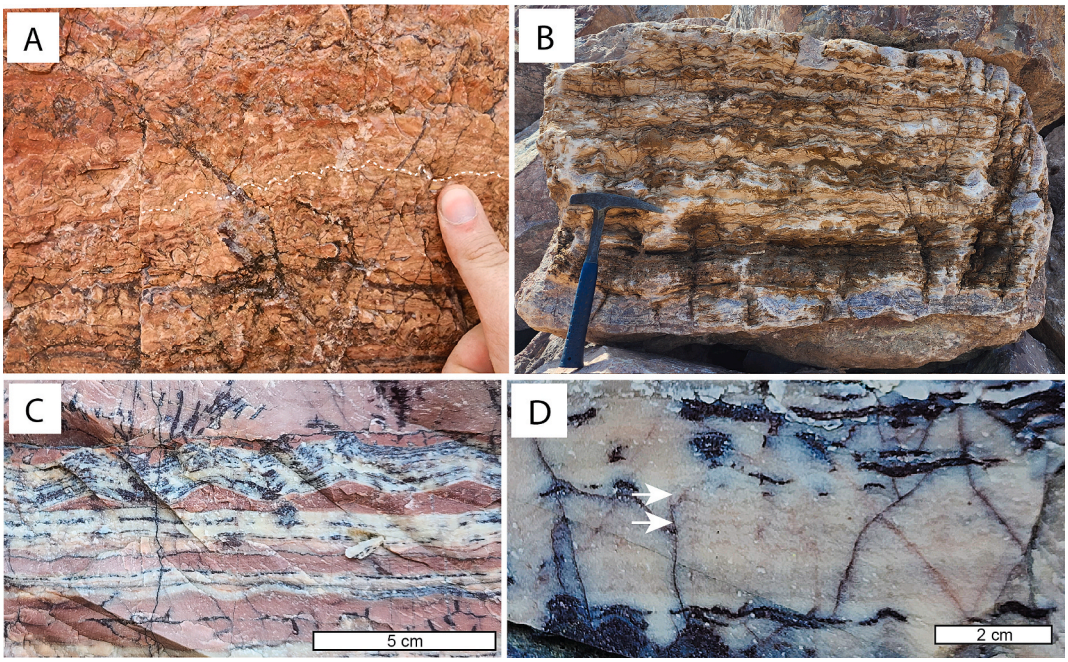

Fig. 4. Stratiform Kona Dolomite stromatolites. A) In cross section at LQ4, millimeter relief and B) Float at LQ1, centimeter sized relief, darker layers are more silicified and lighter layers are more dolomitic, rock hammer is 33 cm tall for scale. C) SLQ3, the red layers are recrystallized dolomite with symmetrical ripple structure with a 2 cm thick mat of stratiform stromatolite inheriting the shape of the ripple marks. D) Adjacent to layering in C, millimeter- scale crinkled layers in former microbial colonies.

4.1.1.2. Domal. Domal morphology is the most common type of stromatolite observed (Figs. 5, 6). Nearly all locations had domes with the exception of LQ4, which is dominated by stratiform stromatolites. The domes are characterized by higher inheritance and relief between microbial lamina, with laminae pinching out towards the bottom of the stromatolite. Domes and columns are often laterally linked and immediately adjacent, usually wider across than tall. At Lindberg Quarry, domal stromatolites ranged from small centimeter sized domes originating from stratiform layers to broadly arching domes decimeters tall and wide. Lindberg Quarry locality 1 (LQ1) had the highest diversity of stromatolite morphologies. The beginning of the stratigraphic section starts with thin, planar sedimentary bedding, with uniform small domes ~ 2 cm tall by 3 cm wide overlain by stratiform morphology (Fig. 5a). The stratiform layer transitions into larger domes with varying relief. Two large domes observed are adjacent to one another with a clear boundary between them, without interstitial sediment. The adjoining domes have different heights and steepness of lamina. One has a relief of ~ 5 cm and a width of 40 cm. The adjacent stromatolite on the right is not completely preserved, but the visible margin shows much steeper lamina with at least 10 cm of relief (Fig. 5c). Stratigraphically above, bedding becomes planar and flat again before transitioning into smaller undulatory and irregular domes, with low inheritance between lamina (Fig. 5b). Lateral transitions from planar to undulatory texture are observed in this bed, and underlie oblong, cyclical microbial morphologies (Fig. 6b,c). South Lindberg Quarry (SLQ1) has broad, low relief domal stromatolites, with pervasive microbial beds of alternating layers of chert and dolomite.

Domal stromatolites at the Highway 480 outcrop (480) are characterized by wide tabular domes, with the largest one about 25 cm tall by 50 cm wide (Fig. 5d). Internally, the domes are made of thin, millimeter thick crinkled layers of chert, and millimeter to centimeter thick layers of dolomite. Stromatolites at 480 are also abundant with rhombal, centimeter sized, red dolomite crystals within and between crinkled lamina. The domal rich bed at 480 is between dolostone mudstone layers with gypsum pseudomorphs and mudcracks, with the very top of the section capped by sandstone. Mount Mesnard domal stromatolites differ from Lindberg quarry stromatolites with wavier and wider stromatolites. Domes across the MM localities range from 3 cm tall by 6 cm wide to 3 cm tall by 55 cm wide, and are thoroughly silicified (Fig. 8b).

4.1.1.3. Roll-up Structures. Roll-up structures are unique to LQ1 and LQ2. The structures are oblong shaped with smooth laminae margins on the outside of the roll-up structure and crinkled internal laminae margins. Whole roll-up structures average a width of ~ 25 cm and height of ~ 6 cm (Fig. 6c). Roll-up structures are composed of thicker bands of pale, pure dolostone and darker, chert-rich dolostone. Internal lamination is more visible in darker dolostone layers, and is usually smooth to wavy in texture. In roll-up structures, the outermost layer curves inward in an oblong, continuous spiral. The spiral terminates near the center of the roll-up structure, typically in a sharp, rectangular edge. Roll-up structures are associated with other types of stromatolites. At LQ1, irregular, undulatory domal stromatolites underlie roll-up rich layers and at LQ2, roll-up structures overlie flat layered dolomite.

4.1.2. Layered dolostone and layered dolostone and chert

Layered dolostone units were present in all recorded localities, ranging from 0.1 m to 2.2 m thick. Layered dolostone has tan-pink and darker red layers and laminations made of microcrystalline dolomite. The dolostone is often interlayered with chert, forming beds between 0.6 and 1.2 m thick. The light pink and tan layers are made of dark red, gray, and white microcrystalline chert (Fig. 7a). The layered chert and dolostone lacked primary sedimentary features but showed secondary alteration like enlarged rhombic dolomite crystals and fractures throughout.

Sedimentary characteristics in layered dolostone include rare cross bedding and gypsum pseudomorphs (Fig. 7b and Fig. 10). Although not in situ, defined symmetrical ripple structures were located on planar beds in float near LQ1 (Fig. 7c). Within LQ1 and LQ2 there is a general trend of parallel flat dolostone layers at the bottom beds, and transitioning to wavier, more stromatolite-rich bedding in the rock face. Locality SLQ3 recorded symmetric undulations in cross-section about 1 cm tall by 10 cm across made of dolostone, which we interpret as ripple

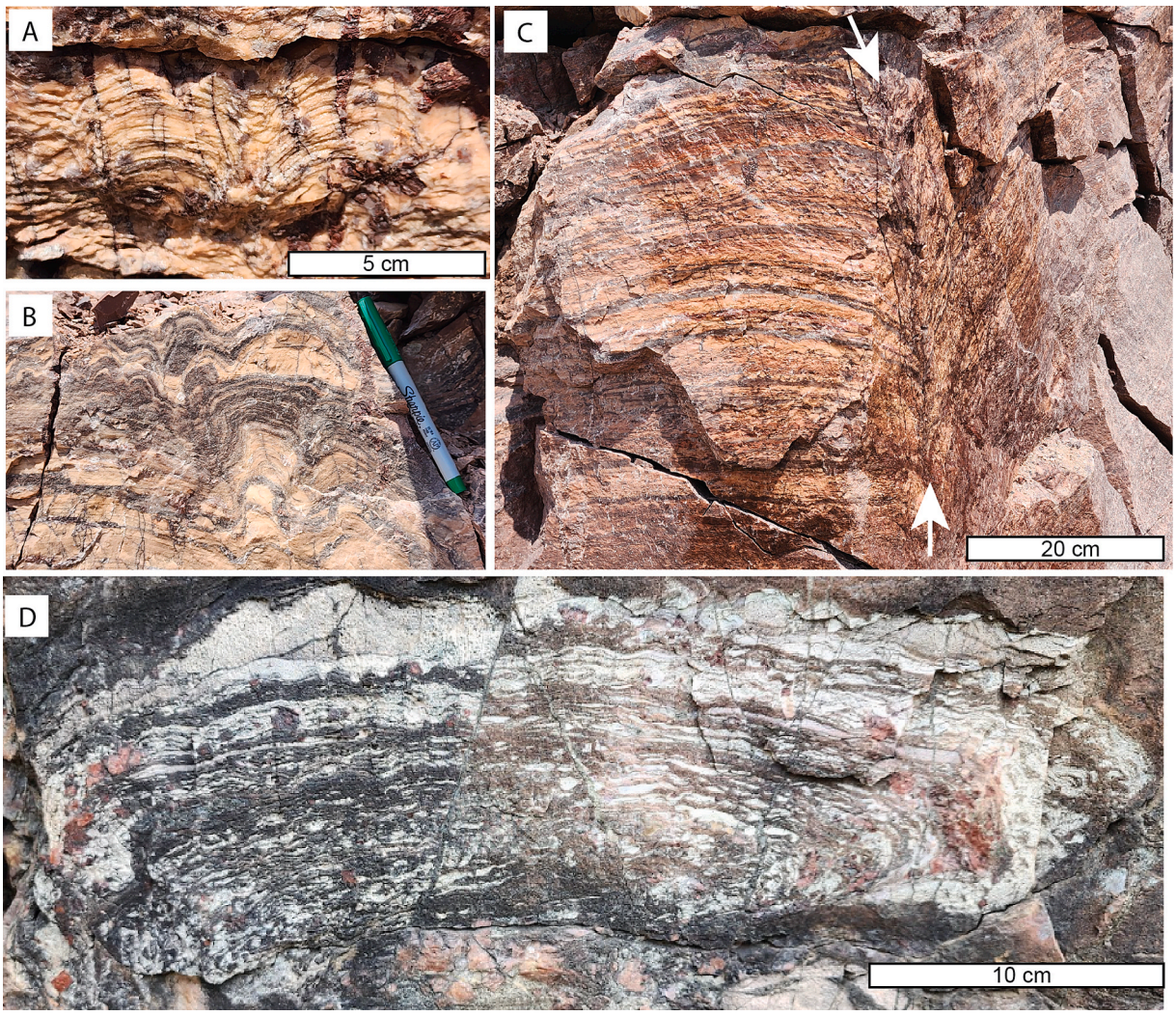

Fig. 5. Domal stromatolites. A) Lindberg Quarry (LQ1) domal stromatolites in cross section, about 2 cm high and 3 cm across for each dome, high inheritance. B) Domal stromatolite at LQ1 further up the stratigraphic section, second order domes and low inheritance of layers. The pen is 15 cm for scale. C) Two adjoined domal stromatolites in the middle of the stratigraphic section at LQ1 with differing reliefs by about 5 cm. Arrows mark the boundary between domes, with the right dome incompletely preserved. D) Domal stromatolite at the highway 480 locality (HWY 480), 25 cm tall by 40 cm wide, the domal stromatolites at this locality are described as tabular, and have secondary small red dolomite crystals throughout the dome.

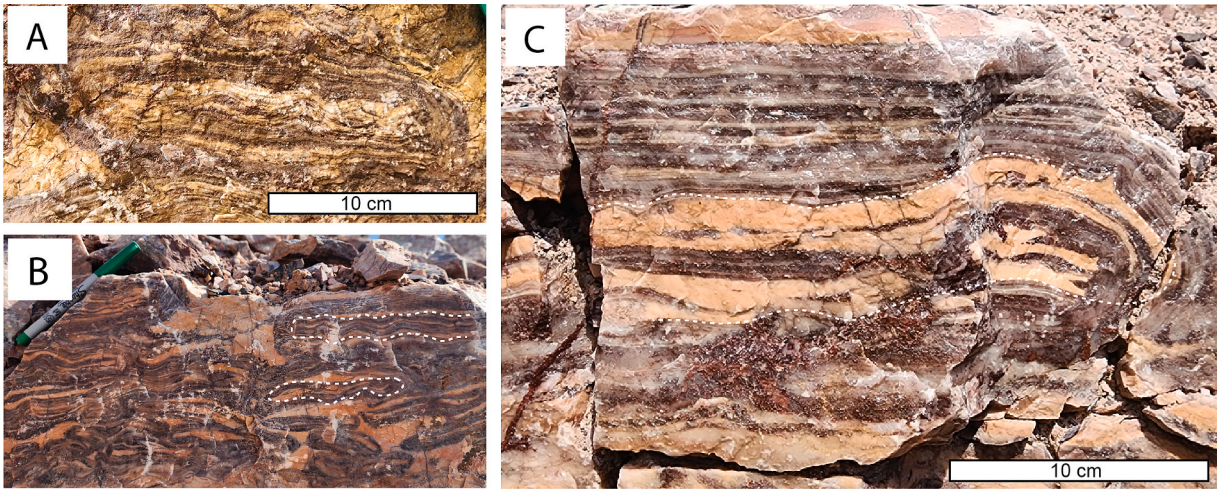

Fig. 6. Roll-up structures: All images in cross section. A) Roll-up structure at LQ2, 30 cm wide by 10 cm tall. B) Roll-up structures at LQ1, pen is 15 cm for scale. C) Incomplete roll-up structure at LQ1, measured section ~ 20 cm long and 10.5 cm tall.

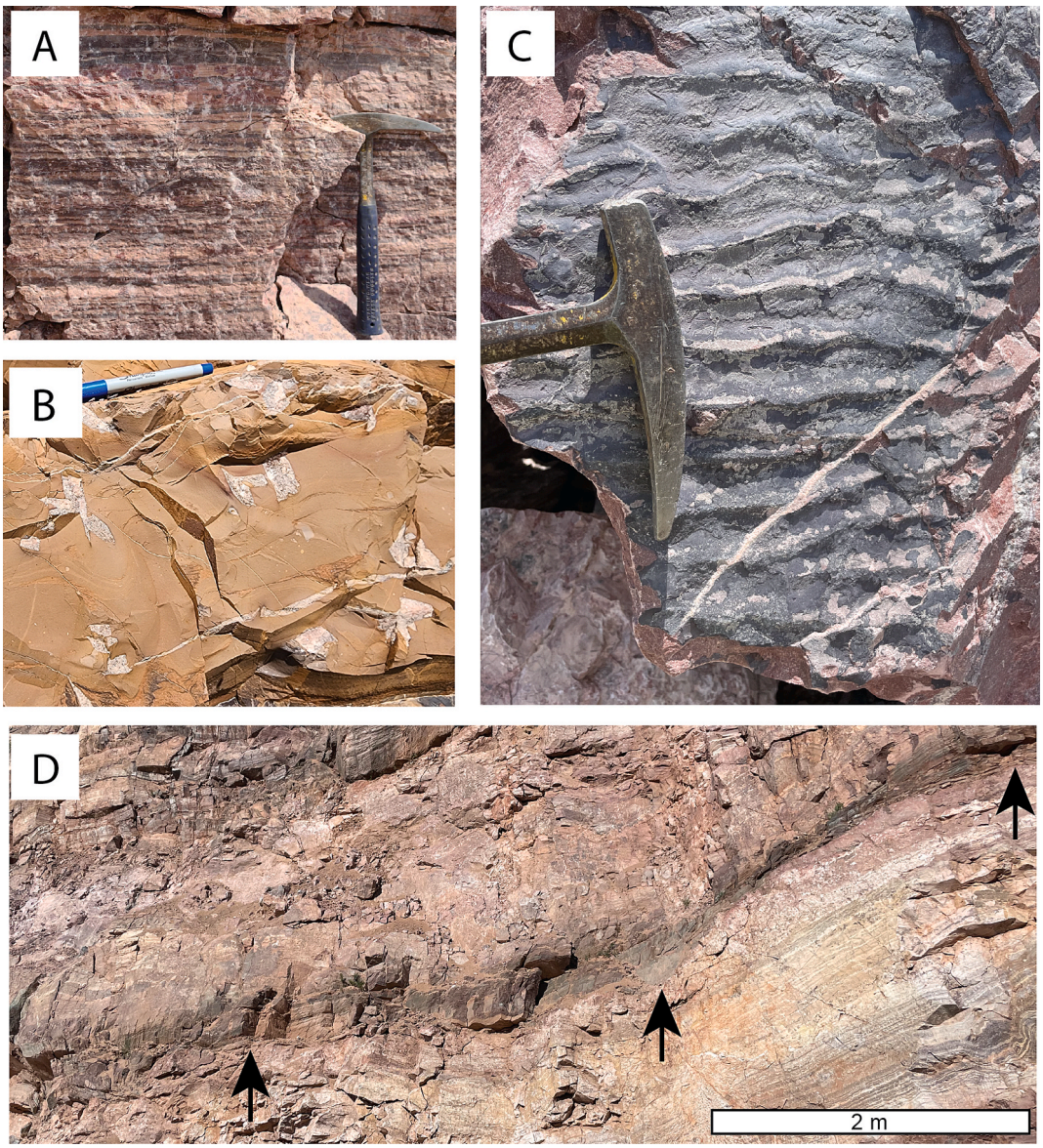

Fig. 7. Sedimentary features of the Kona Dolomite: A) Layered microcrystalline chert (gray) and microcrystalline dolomite (pink) at LQ1, rock hammer for scale. B) Gypsum pseudomorphs at HWY 480, varying rhombus shapes ~ 1–10 cm in size, towards the base of the section. The pen is 15 cm for scale. C) Symmetrical ripple marks in float at Lindberg Quarry, Head of rock hammer for scale. D) Unconformity at Lindberg Quarry, above measured sections.

marks (Fig. 4C). Stromatolites with mm-scale laminations are deposited directly on top, inheriting the underlying undulations (Fig. 4C). Gypsum pseudomorphs are common at Lindberg quarry and 480, ranging about 1–10 cm in length and height (Fig. 7b). The pseudomorphs replaced distinctive shapes such as rosettes, rhombus squares, and swallowtail twinning. Mudcracks are also preserved at the base of 480 within the layered mud-dolostone.

4.1.3. *Structureless dolostone*

Wholly recrystallized dolostone beds are present at the LQ1, LQ4, and Highway 480 sites, and are thinner than other beds (0.15–0.4 m thick). Typically light in color and massive, the recrystallized dolostone has little to no original features, though evaporite pseudomorphs are visible in the Highway 480 section (Fig. 7B). In other localities these beds often have red dolomite crystals and may have been subject to more metamorphism and secondary alteration than the other beds.

4.2. *Petrography*

Stratiform and domal stromatolites are composed of carbonate layers with varying crystal sizes: micrite (<4 μm), microspar (4–20 μm), and some isolated sections of spar or enlarged dolomite rhombs (>20 μm). Stratiform stromatolites are made of micrite layers up to 1 mm thick and microspar layers up to 0.5 mm thick (Fig. 9a). Layers in domal stromatolites had alternating micrite layers 2 mm thick and microspar-spar layers 0.5 to 1 mm thick. In one thin section, LQ 1–2, there was a rounded clast of micrite covered by fine laminations of micrite and microspar (Fig. 9b). Samples had matrix of spar and quartz, ranging from 10% to 50% quartz. Quartz in Kona Dolomite samples is predominantly cement, forming in veins or pseudomorphs. Pseudomorphs are rare in thin sections, forming distinct rosettes of elongated radiating crystals (Fig. 10C). In rare, discontinuous layers ~ 1–5 mm thick, subrounded to subangular quartz grains are observed between thicker, quartz-poor dolomicrite layers. Some areas in the thin sections had structureless, plain layers of micrite, and others had layers of micrite and microspar displaying domal structures. SLQ1-1 had occasional, localized

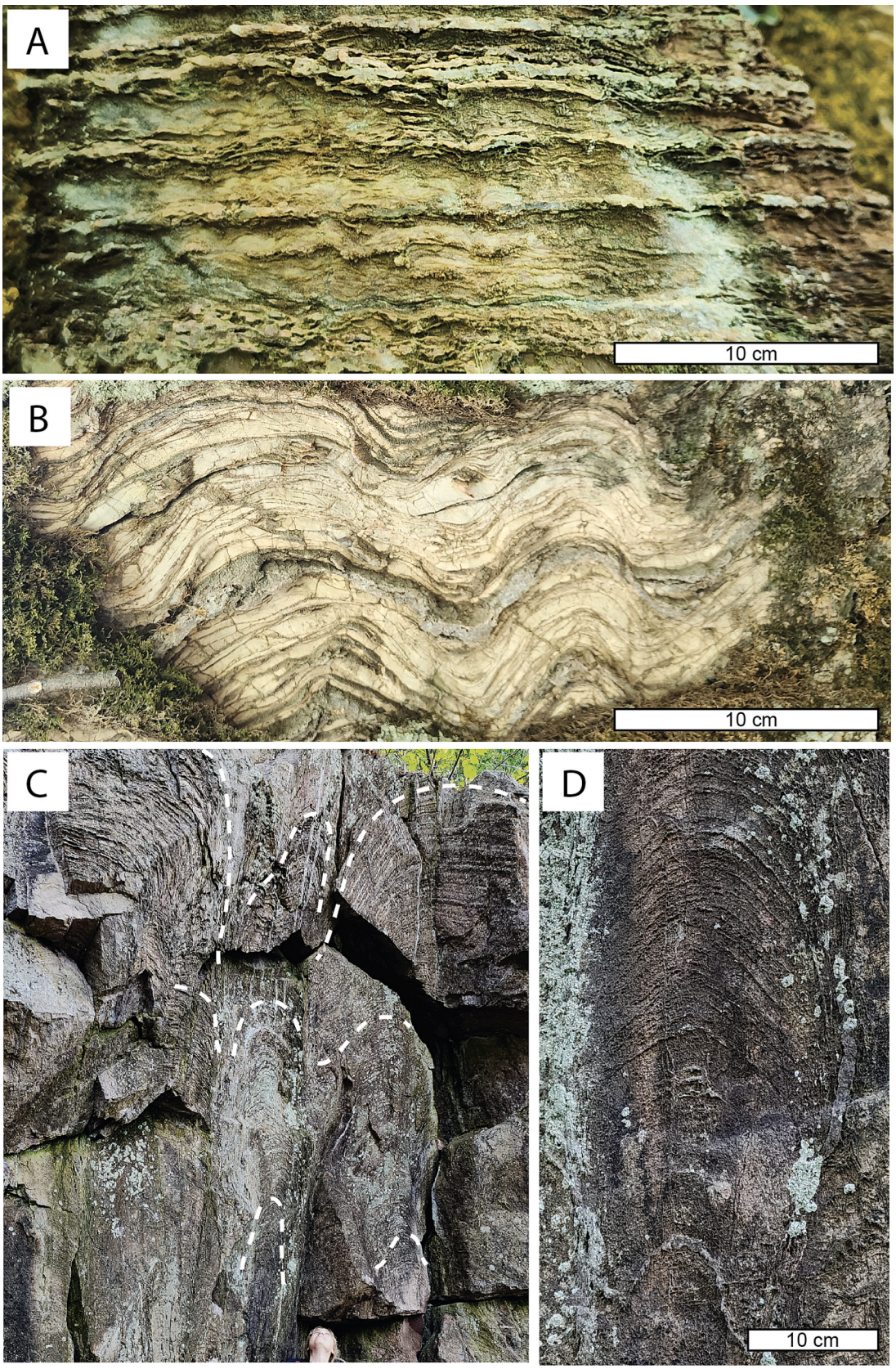

Fig. 8. Stromatolites from eastern Marquette (Mount Mesnard and Lakeshore localities): A) Stratiform stromatolite at MM2, millimeter sized relief, the more resistant layers are made of chert. B) Domal stromatolites at MM2, centimeter sized relief and wavy domal texture that continues laterally. Domal Stromatolites on Lake Superior: C) Large domal stromatolites at the Lakeshore locality, 9 m tall by 50 cm wide, 20 cm of relief between layers. D) Domal stromatolite 60 cm tall by 20 cm wide, ~10 cm of relief between layers.

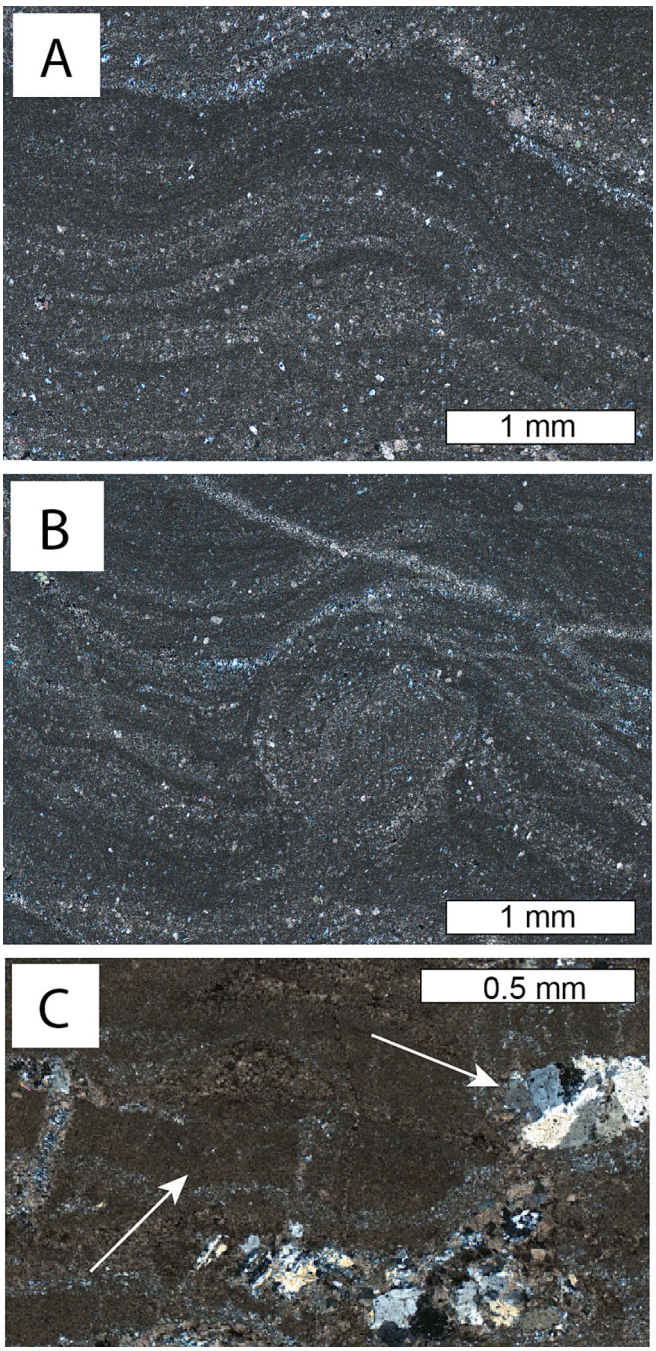

Fig. 9. Microbialite and laminated dolomite petrography: All images in XPL. A) Stratiform stromatolite, micrite layers 2 mm thick and microspar spar layers 0.5 to 1 mm thick. B) Rounded clast surrounded with fine laminations of micrite and microspar. C) The left arrow shows millimeter sized micrite carbonate clasts with interstitial microspar matrix. The right arrow points to quartz rich pockets that were likely formed during diagenesis and infiltration of siliceous fluids.

layers with millimeter sized, radiating planar subhedral crystals filled with quartz. (Fig. 10c, Supp. Fig. S1). LQ1-1 has layered and scattered fine sand-sized grains made of quartz throughout the thin section; no other samples had identifiable sand grains. Sand layers were no more than 0.25 mm thick and alternated with micrite.

Later on, diagenesis and metamorphism altered features of the rocks, causing recrystallization. In samples from SLQ and MM, macroscale microbial textures have crinkled, irregular laminae, but were recrystallized in thin sections. Quartz veins and replacement of primary minerals are common in all samples (Fig. 9c), especially in the Mount Mesnard thin sections. At locality 480, pseudomorphs 1–4 cm long are scattered throughout the massive dolostone layer, filled with quartz. Pseudomorphs are typically clustered together and demonstrate rhombic, rosette, and swallowtail morphologies (Fig. 7B). All samples had secondary iron staining following veins, fissures, and infiltrating spar, microspar, and micrite layers. Red hematite often stains micrite matrices (Fig. 10b), giving samples a pink-purple coloration. Tremolite veins and needles are present and scattered throughout most samples (making up < 5% of the thin section) (Fig. 10a).

4.3. Geochemistry

Samples from the western Kona (LQ, SLQ, 480) and eastern Kona (MM) have a similar isotopic range and trends (Fig. 11, Table 2). Across the Kona, values of $\delta^{13}C$ ranged from + 3.8‰ to + 8.6‰, while $\delta^{18}O$ ranged from −6.7‰. to −14.0‰. In western Kona, $\delta^{13}C$ varies from + 4.9‰. to + 8.4‰, and $\delta^{18}O$ between −6.7‰. and −13.6‰. In eastern Kona, $\delta^{13}C$ varies between + 3.8‰ and + 7.9‰, and $\delta^{18}O$ varies between −7.3‰. and −14.0‰. When examining all Kona Dolomite samples, there is no correlation between $\delta^{13}C$ to $\delta^{18}O$ (Fig. 11A, r2 = 0.07). However, removing three clusters of datasets from samples SLQ1-1, LQ1-2, and MM3 greatly increases the correlation coefficient between $\delta^{13}C$ and $\delta^{18}O$ (r^2 = 0.9). There is broad isotopic overlap between sampled facies of planar dolomite, stratiform stromatolites, and domal stromatolites, with and without evaporite pseudomorphs (Table 2, Supplemental Fig. S1). In planar dolomite without evaporative pseudomorphs, $\delta^{13}C$ ranges between + 4.9‰ to + 6.9‰ and $\delta^{18}O$ between −9.8‰ and −13.2‰. In planar dolomite with evaporative pseudomorphs, the $\delta^{13}C$ and $\delta^{18}O$ range decreases, with $\delta^{13}C$ between + 5.8‰ to + 6.0‰ and $\delta^{18}O$ between −11.3‰ and −11.4‰. Overall, $\delta^{18}O$ tends to be lower (below −9.5‰) in planar dolomite than other facies. Stratiform stromatolites without evaporative pseudomorphs have a $\delta^{13}C$ range of + 6.2‰ to + 6.5‰, and $\delta^{18}O$ range of −10.8‰ to −11.6‰. Stratiform stromatolites with evaporative pseudomorphs have a broader range, with $\delta^{13}C$ between + 4.9‰ and + 8.4‰ and $\delta^{18}O$ between −6.7‰ and −10.4‰. In contrast to planar dolomite, values of $\delta^{18}O$ tend to be higher in stratiform stromatolites (above −12‰). Domal stromatolites have the widest range of isotopes, with $\delta^{13}C$ occurring between + 3.8‰ and + 7.9‰, and $\delta^{18}O$ between −7.3‰ and −14.0‰ (Supplemental Fig. S1).

Mn/Sr ratios in powders ranged from 1 to 54, with Mn ranging from 217 to 2390 ppm and Sr ranging from 36 to 390 ppm (Fig. 11, Table 2). In the western Kona, Mn/Sr ratios ranged from 2 to 54, with Mn ranging from 468 to 2390 ppm and Sr ranging from 37 to 224 ppm. In eastern Kona, Mn/Sr ratios ranged from 1 to 52, with Mn ranging from 217 ppm to 2302 ppm and Sr ranging from 36 ppm to 390 ppm. Uncertainties for elemental measurements were better than two percent of measured values. There are no clear trends between $\delta^{13}C$ and Mn, Sr, or Mn/Sr (Fig. 11), and no significant difference between western and eastern samples.

5. Discussion

5.1. Depositional environment

Kona deposits across Marquette were initially described as “shallow marine” (van Hise & Bayley 1895; Gair & Thaden, 1968; Puffett 1974; Gair 1975), with limited discussion of facies or stratigraphy. The most extensive study of Kona sedimentology is an unpublished doctoral thesis (Taylor 1972), mapping 11 members across the entire syncline using Mount Mesnard as a type section. While these members have been used as frameworks for subsequent studies (Wohlabaugh & Mancuso, 1990; Bekker et al., 2006; Ramsay et al., 2025), they remain informal, and no study has verified Taylor 1972′s initial interpretations on a basinwide scale.

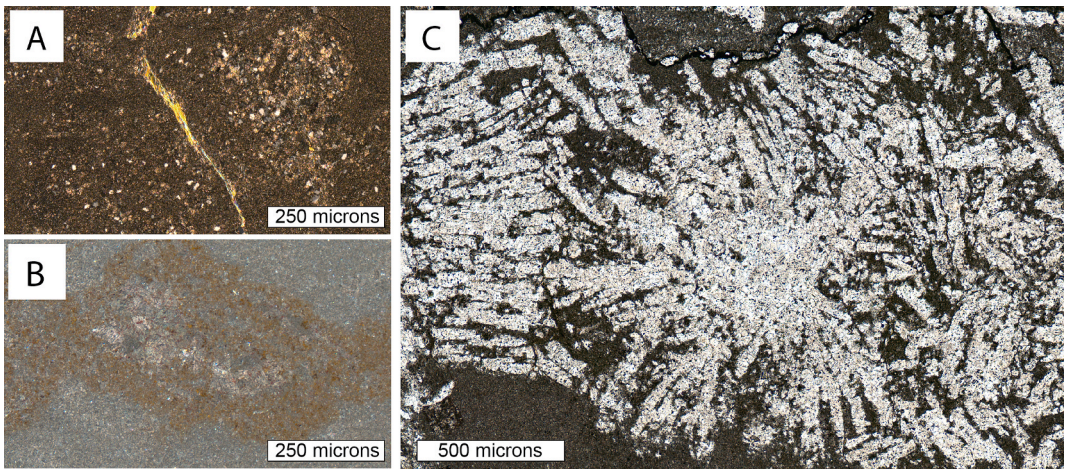

Fig. 10. Secondary alteration and gypsum pseudomorph petrography. All images in XPL: A) Tremolite vein in microspar matrix. B) Iron staining in micrite matrix under reflected light. C) Gypsum pseudomorphs from SLQ1, rosette needles replaced by quartz in micrite matrix.

5.1.1. Evaporative and peritidal facies

Pseudomorphs of sulfate minerals (gypsum or anhydrite) were observed at the Highway 480 locality as large rhombs in structureless dolostone (Fig. 7b), and under thin section as rosettes in stratiform stromatolites from South Lindberg Quarry (SLQ1-1). In Taylor (1972), the 480 site was interpreted as Member 11, at the top of a major exposure of westward-dipping Kona Dolomite in the Lindberg Quarry Region (Fig. 2a). If true, this study extends the record of evaporitic sulfate deposition much later than previous studies, to the uppermost Kona Dolomite. Taylor (1972) reported similar sulfate pseudomorphs (blades and rosettes) and square casts of halite in lower clastic members (members 1, 2, and 4), but not in the upper dolostone members. Taylor interpreted pseudomorph-rich lower members as an evaporative bay restricted by a land barrier, followed by an open tidal ramp after Member 5 (Taylor 1972, Fig. 12).

Subsequent discoveries of gypsum pseudomorphs in Member 6 revealed that evaporitic conditions persisted into lower dolostone units (Wohlabaugh & Mancuso, 1990). Member 6 was compared with modern evaporitic sabkhas in Western Australia and the Persian Gulf, with gypsum pseudomorphs indicating periods of higher salinity (Wohlabaugh 1980, Wohlabaugh & Mancuso 1990). New pseudomorph locations from this study indicate that intermittent evaporation extended later into Kona deposition than previously described. In particular, this is the first study to describe evaporative gypsum pseudomorphs as stratigraphically high as member 11. Rather than a distinct shift from evaporite-rich clastics to evaporite-poor dolomites, Lindberg Quarry exposures reveal that evaporation occurred intermittently throughout Kona history.

Other evidence for subaerial exposure comes from unconformities. At LQ4 (Member 10), a low-angle unconformity within the Kona Dolomite was observed high in the quarry wall above the measured stratigraphic column (Fig. 7d). Unconformities of similar scale were also described in South Lindberg Quarry by Larue (1981), based on irregular weathering surfaces in hand samples. Both lines of evidence were interpreted as periods of regression and erosion of supratidal mud and sediments. While faulting occurs in Kona deposits, the unconformities are not interpreted as tectonic in origin (i.e., thrust faulting), due to the lack of immediately associated deformation in under- or overlying deposits (Fig. 7d). The specific members for unconformities and weathering surfaces were not noted, but their presence in thick dolomite-rich layers from Lindberg Quarry implies extensive subaerial exposure later in Kona deposition, in contrast with earlier interpretations (Taylor 1972). Mud cracks have also been described in Kona deposits (Taylor 1972; Larue 1981). also indicating periods of exposure. Together, these features suggest that subaerial exposure was more widespread and recurrent during Kona Dolomite deposition than previously recognized.

Low-relief, stratiform stromatolites were abundant in many measured stratigraphic sections (Fig. 4), including samples with interbedded pseudomorphs of sulfate rosettes (Fig. 7b). In modern and ancient environments, stratiform stromatolites are indicative of shallow peritidal environments such as tidal flats and sabkhas (Fig. 12), forming crinkled layers typically less than one cm in relief (Logan et al., 1964; Hofmann 1975; Beukes & Lowe, 1989; Southgate 1989; Kah & Knoll, 1996; Altermann 2008; Jahnert & Collins 2012). Such layers indicate that more frequent tidal influx had to occur to stimulate microbial growth. Based on the evidence above, periodic exposure then led to intermittent evaporite precipitation and cessation of stromatolite formation.

5.1.2. Intertidal facies

Living microbial mats are cohesive organo-sedimentary structures, bound by filamentous cells and adhesive compounds such as extracellular polymeric substances. When disturbed by outside energy such as waves or wind, microbial mats deform in unique patterns that are difficult to replicate with abiotic sediments alone. For example, “roll-up structures” occur when a flat or low-relief mat is partly removed from its underlying substrate by a wave or storm (Simonson & Carney 1999; Hagadorn & McDowell 2012). If the mat is particularly cohesive, the “loose” detached margin will fold over adjacent, undisturbed planar mats, forming a continuous curve much like a folded carpet (Fig. 6c). Especially powerful disturbances can repeat this process, folding mats into spirals or sinuous curves.

This study provides the first description of microbial roll-up structures from the Kona Dolomite. The structures were only observed in columns LQ1 and LQ2, on the eastern edge of Lindberg Quarry. According to Taylor (1972) both localities are part of Member 10 (“Ragged Hills Dolomite”). Such roll-up structures form in the intertidal zone, where there is more wave activity which disturbs and moves sediments. The abundance and meter-scale size of the roll-up structures indicates that 1) the disturbances were strong enough to disturb thick, indurated microbial mats, and 2) the mats had ample time to grow extremely cohesive colonies over 1 cm thick before the disturbance. Such evidence indicates infrequent storm activity as opposed to regular wave disturbance, either deposition in the lower intertidal zone or in a protected lagoon (Fig. 12). The deposits underneath roll-up layers were flat layers of dolostone and chert, or stratiform stromatolites. In these regions, wave energy may have changed frequently, as well as relative water depth, creating disturbed stromatolite structures on otherwise calm deposits. It is possible the two localities represent the same storm event, but distance and cover prevents correlation between the two columns,

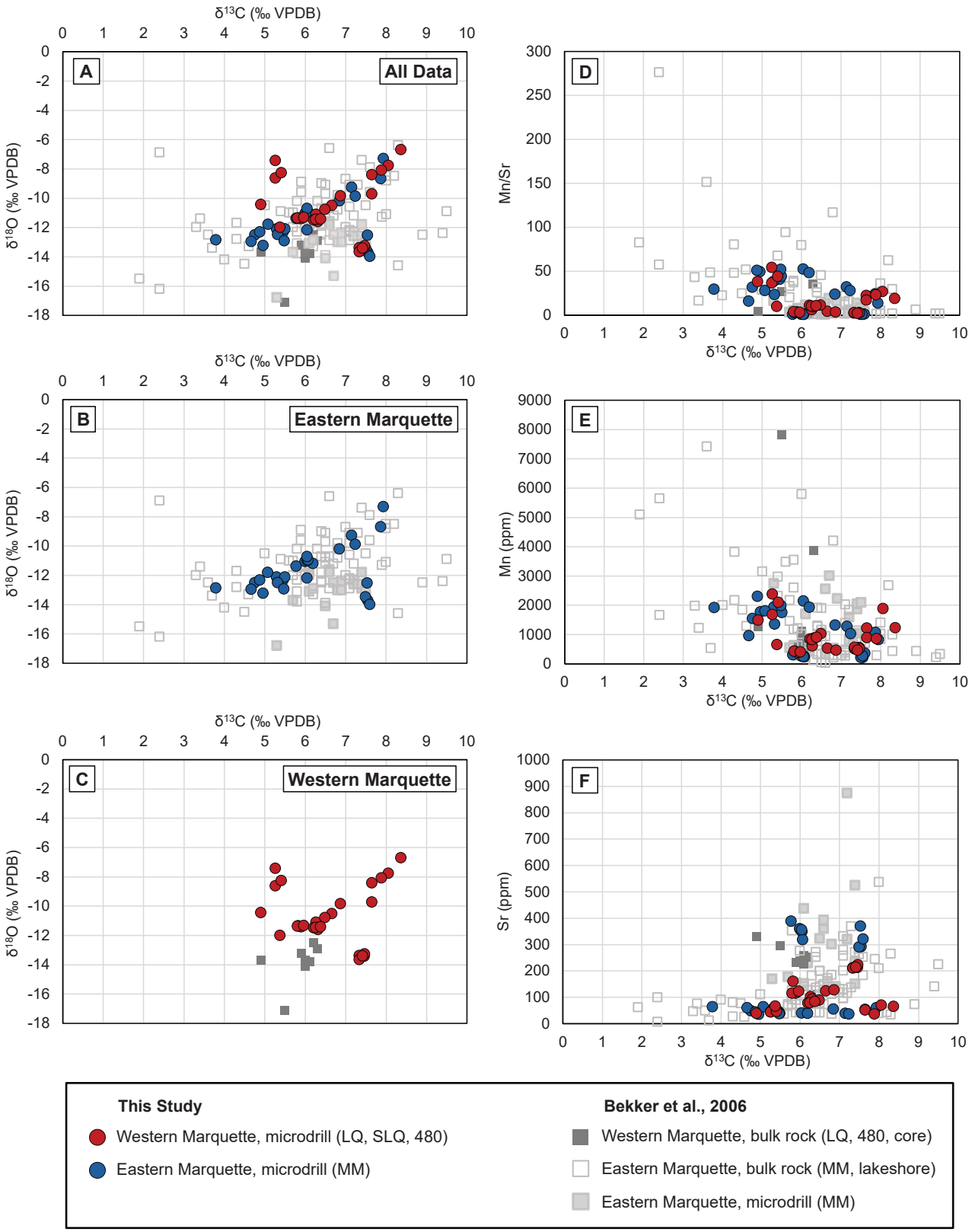

Fig. 11. Carbon and oxygen isotopes in the Kona Dolomite. A: All published measurements from the Kona Dolomite, highlighting new data from this study. B: Current and previous measurements from eastern Marquette. C: Current and previous measurements from western Marquette. D: $\delta^{13}C$ vs. Mn/Sr ratios from this study and Bekker et al., 2006. E: $\delta^{13}C$ vs. Mn concentrations from this study and Bekker et al., 2006. F: $\delta^{13}C$ vs. Mn concentrations from this study and Bekker et al., 2006.

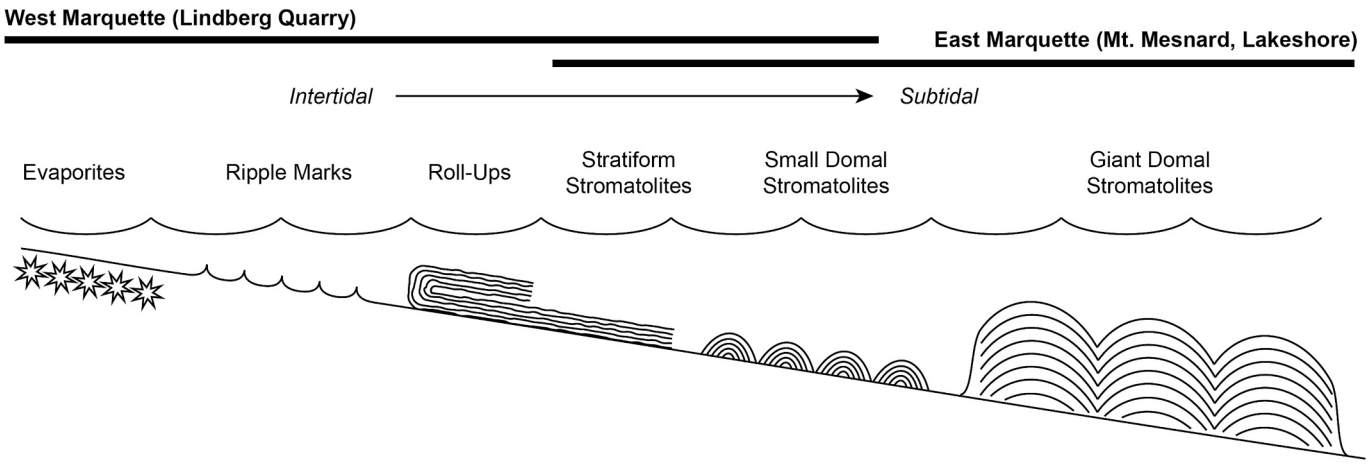

Fig. 12. Profile of sedimentary features and interpreted depositional environments in the Kona Dolomite, from western to eastern Marquette.

and they are conservatively interpreted as two distinct events.

Among the measured stratigraphic columns, cross-bedding and ripple marks are relatively rare in the Lindberg Quarry area. Previous studies only noted cross-bedding in interbedded quartzites and argillites rather than dolomites (Taylor 1972; Wohlabaugh 1980: Larue 1981). As clastic deposits were rarely observed in this study, the relative lack of cross-bedding in several meters of peritidal and intertidal facies is not considered abnormal, especially considering the abundance of cohesive mats forming stromatolite beds. At SLQ3, dolostone ripple marks were found with a stratiform microbial mat on top, taking on the shape of the underlying ripple marks (Fig. 4C). The interaction indicates alternating periods of wave action creating ripple marks, and calmer environments allowing stromatolites to form. Such patterns corroborate the periodic disturbances necessary to form roll-up structures, though on a more subdued scale. Other than the stromatolite-covered ripples in SLQ, ripple marks were only observed on a single piece of quartzitic float at Lindberg Quarry (Fig. 7c).

5.1.3. *Lateral facies variations*

The abundance of evaporites in western Marquette and their relative scarcity in the east supports previous interpretations of a western shoreline, with waters deepening to the east (Fig. 12). Further evidence for shallower western facies include 1) dm to m-scale microbial roll-up structures, 2) ripple marks, and 3) an abundance of crinkled stratiform stromatolites. None of these features were observed in eastern Kona exposures, though as noted, eastern outcrops have become less well-preserved. Instead, the majority of eastern Kona outcrops contained domal stromatolites (Figs. 5, 12). Of these, the most notable are the giant stromatolites on the Lake Superior shoreline (Twenhofel 1919) which measure up to 9 m high by 50 cm wide with a relief of about 20 cm (Fig. 8C, D). These large lakeshore domes are wide across, vertically pervasive, and had a high relief from the seabed. Domal stromatolites are typically interpreted as intertidal to subtidal, with larger domes requiring more accommodation space (Logan et al., 1964; Shapiro & Wilmeth, 2020). Therefore, the presence of giant domal stromatolites in the easternmost Kona, contrasted with evaporites, roll-up structures, and stratiform stromatolites in the west, strengthens the interpretation of a westward-shallowing embayment for Kona deposition (Fig. 12).

The Kona Dolomite around Lindberg Quarry was deposited in supratidal sabkhas and shallow tidal flats. Cohesive microbial mats did not frequently form ripples, but produced roll-up structures when disturbed by larger storm events. Deeper and calmer periods allowed domal stromatolites to grow, while subaerial exposure produced evaporites and unconformities (Fig. 7b,d). In the east, Mount Mesnard and the Lakeshore locality have evidence for a relatively deeper and calmer marine environment, forming in the lower intertidal to subtidal zone. No evidence was observed for energetic waters, gypsum precipitation, or stratiform stromatolites. Instead, eastern Marquette contains the largest stromatolite domes and columns in the Kona Dolomite (> 1 m high), likely forming in relatively deeper undisturbed water.

This study confirms previous sedimentary analysis of a deepening trend from west to east in the Kona. Similar evaporite pseudomorphs were also described by Taylor 1972, Wohlabaugh 1980, and Larue 1981. In these studies, the only specific evaporite localities mentioned are from Lindberg Quarry and adjacent drill cores in western Marquette (Wohlabaugh 1980, Larue 1981). Taylor 1972 mentions abundant evaporites in lower clastic members (Members 1–5), but unfortunately does not mention specific locations. The most logical locality for these lower evaporites would be Taylor's type section of Mount Mesnard in eastern Marquette, but they remain unconfirmed by other research. This study did not find evaporite pseudomorphs in eastern Kona deposits, though available outcrops were limited. Previous studies of the Kona Dolomite and other formations in the Marquette area indicate a transition from deeper waters in the east to a shallow shoreline in the west (Fig. 12). Evidence for westward shallowing comes from cross-bedding in quartzites (Tyler & Twenhofel 1952; Pettijohn 1957), sedimentary units pinching out to the west with increasing brecciation (Taylor 1972), and wave-driven stromatolite orientation (Wohlabaugh & Mancuso 1990). New evidence such as evaporative pseudomorphs in later stratigraphic members, documentation of roll-up structures and other disturbed microbialites at Lindberg Quarry, and larger stromatolites in the west show that there was a lateral environmental change across the Kona Dolomite. While the localities in this study are not directly correlative, comparing western and eastern Kona sedimentology corroborates previous interpretations and provides further detail on facies distributions.

5.2. *Geochemistry*

Isotopic data from this study expand and complement previous datasets measured by Bekker et al., 2006 (Fig. 11), and recently by Ramsay et al., 2025. The 2006 study focused on the Mount Mesnard area as the type locality from Taylor 1972. Of 112 Kona samples analyzed by Bekker et al., 2006, the majority came from eastern Marquette (101 from Mount Mesnard, 2 from the Lakeshore locality), while 10 came from western Marquette (4 from Hwy 480, 3 from Lindberg Quarry, 1 from drill core in the same area), with one sample of unlisted origin (Figs. 2, 11). Most recently, Ramsay et al. 2025 recently described the Kona Dolomite along with the Gordon Lake Formation, analyzing $\delta^{13}C$ among different stromatolite morphologies and different sedimentary facies, plotting a similar cloud without clear correlation of carbon and oxygen isotopes. Our study adds to these datasets, particularly in western

Marquette (Fig. 11), with 60 new microdrilled samples (30 from the west, 30 from the east).

5.2.1. Covariance and alteration

The most notable feature of our dataset is a strong positive covariance between $\delta^{13}C$ and $\delta^{18}O$ (Fig. 11A), which can be diagnostic of secondary alteration by meteoric fluids or in their subsurface mixing zones with seawater (e.g., Allan & Matthews 1982; Calver 2000; Melim et al., 2004; Swart & Oehlert 2018). The main body of isotopic data extends from depleted values in sample MM1 ($\delta^{13}C$: 3.8‰, $\delta^{18}O$: −12.8‰ VPDB) to the highest values in sample SLQ1-1 (δ13C: 8.4‰, $\delta^{18}O$: −6.7‰ VPDB) (Fig. 11A, Table 2). Three hand samples with nine analyses clearly diverge from this positive correlation: SLQ-1–1 ($\delta^{13}C$: ~5.3‰, $\delta^{18}O$: ~-8.0‰), and LQ1-2 and MM3 ($\delta^{13}C$: ~7.4, $\delta^{18}O$: ~-13.4) (Fig. 11A, Table 2). Without these outliers, the main body shows high covariance ($r^2 = 0.88$). However, with all data included, covariance becomes nearly negligible ($r^2 = 0.07$), more closely matching $\delta^{13}C$ vs. $\delta^{18}O$ from Bekker et al., 2006 ($r^2 = 0.07$, Fig. 11B). Our isotopic data falls well within previously measured ranges (Fig. 11E) using similar microdrilling techniques (Bekker et al., 2006). Another recent set of stable isotope measurements from the Kona Dolomite also reveals no isotopic correlation between $\delta^{13}C$ and $\delta^{18}O$ (Ramsay et al., 2025). Therefore, we interpret the apparently high $\delta^{13}C$- $\delta^{18}O$ correlation in the majority (but not all) of our data as a product of multiple measurements from a few individual rocks, compared with studies that sampled more rocks and found no correlation (Fig. 11, Bekker et al., 2006; Ramsay et al., 2025).

Even when regarding the high covariance of our isotopic data as a sampling artifact, the positive trend indicates secondary alteration of the Kona Dolomite. This could take the form of early precipitation of cements in pore fluids, as observed in modern platforms with frequent subaerial exposure to meteoric fluids (Swart & Oehlert 2018; Smith & Swart 2022; Geyman & Maloof, 2021). For example, meteoric alteration and early cementation of shallow Bahamian carbonates over ten thousand years can decrease $\delta^{13}C$ between 1 and 13‰, with smaller but significant decreases in $\delta^{18}O$ (Geyman & Maloof, 2021). While former pore spaces were rarely observed in Kona samples, recrystallization is more pervasive than coeval dolomites in the Lake Superior region (Figs. 10, 11; Brown et al., 2025). Relatively shallow deposition close to evaporative zones increases the likelihood for early meteoric influence in the Kona Dolomite.

The entire formation is also within the low-metamorphism chlorite zone of James (1995) and has been folded into a gently plunging syncline with multiple generations of folds throughout (Gair & Thaden, 1968; Taylor, 1972; Puffett 1974; Gair 1975). The effects of metamorphism and alteration can be observed in both the petrography and geochemistry of hand samples. Tremolite grains appear in clastic-rich samples (Fig. 10A), which can form due to reactions between clastic grains and carbonate minerals above 350 °C (Tilley 1948). Kona Dolomite samples also demonstrate silicification, recrystallization, and fracturing (Fig. 4B, Fig. 5D, Fig. 7A, Fig. 10C, Fig. 11B), though more well-preserved samples can preserve micritic layering (Fig. 9) and fine-scale details such as gypsum rosettes (Fig. 10C).

Petrographic analyses were used to select the least-altered portions of samples (least recrystallized/silicified, micrite-rich, away from fractures or cements), techniques that were also utilized by Bekker et al., 2006. However, tests of isotopic variability within individual samples revealed that such screenings might still be insufficient (Fig. 13). In sample MM3, powder samples were collected from similar horizons ~ 5 cm apart, with varying distance from a silica-rich vein (Fig. 13B). The $\delta^{13}C$ values of powders collected closer to the vein (~1–5 cm), were consistently ~ 1.5‰ higher than powders collected farther away (7–10 cm). Secondary influences in other samples were less clear. Sample MM1 contained $\delta^{13}C$ values between 3.78 and 7.93‰ across 10 cm (Fig. 13A), with no clear trends with veining, silicification, recrystallization or micrite abundance.

Previous Kona Dolomite studies used Mn/Sr ratios to assess the extent of secondary overprint of $\delta^{13}C$ measurements (Fig. 11; Bekker et al., 2006). Alteration from meteoric fluids typically increases Mn concentrations, decreases Sr, and decreases $\delta^{13}C$ (Veizer 1983; Kaufman et al 1993; Kaufman & Knoll, 1995). Therefore, a clear alteration trend would contain isotopically-depleted carbonate with higher Mn/Sr ratios. Kaufman and Knoll (1995) suggested an upper Mn/Sr threshold of 10 for examining Neoproterozoic $\delta^{13}C$, but also noted the threshold was subject to interpretation, since major isotopes are less sensitive to meteoric influence than Sr. For example, Bekker et al., 2006 considered Kona Dolomite samples with Mn/Sr values up to 80 as valid for investigating $\delta^{13}C$.

In our study, Mn/Sr values reached a maximum of 52.2 (Fig. 11D). No correlation exists between $\delta^{13}C$ values and Mn/Sr ratios in our microdrilled samples, or with Mn and Sr concentrations (Fig. 11). In comparison, Bekker et al., 2006 found mild correlations between $\delta^{13}C$ and Mn/Sr ratios in bulk samples, but microdrilled samples also revealed no correlation (Fig. 11D). Sample preparation for Mn and Sr

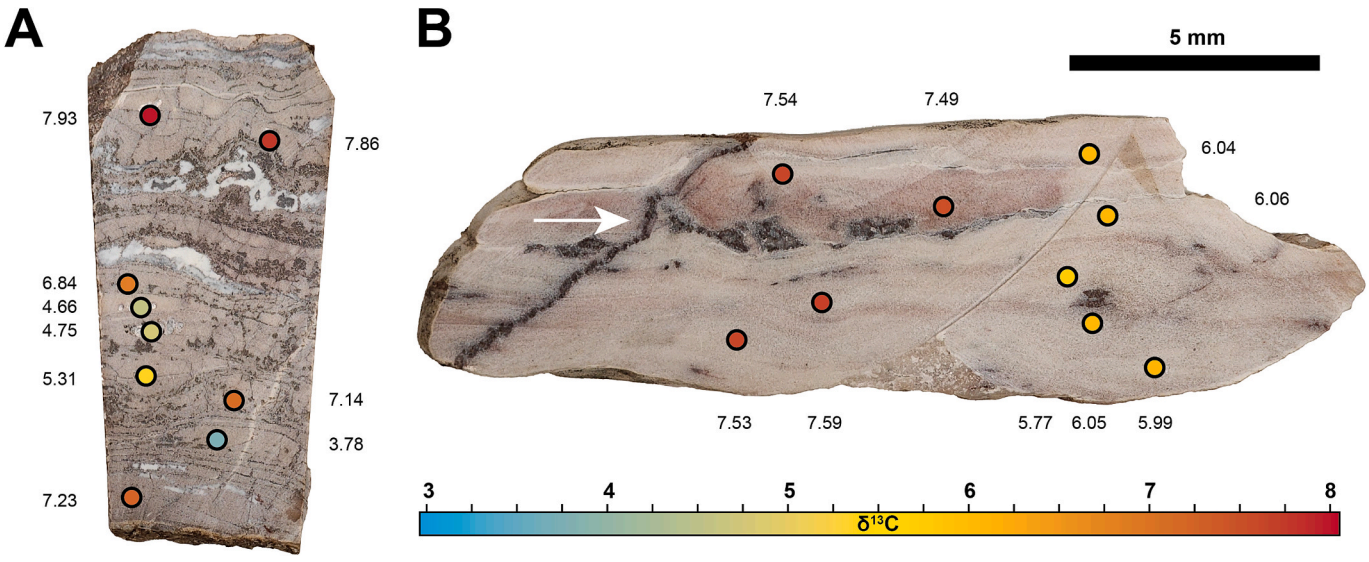

Fig. 13. $\delta^{13}C$ variability within individual samples. Darker layers and veins have higher quartz and chert concentrations. A: Sample MM1. Pure white zones are recrystallized cements. B: Sample MM3. Arrow points to a quartz vein.

followed Bekker et al., 2006's methods on the Kona Dolomite, dissolving microdrilled powders in nitric acid. Such preparations can introduce elements from clastic minerals (Tostevin et al., 2016), potentially accounting for the lack of Mn/Sr correlation, though drill locations were chosen to avoid detrital contamination when possible. While Mn/Sr values from the Kona Dolomite are still inconclusive, they highlight the need for more targeted preparation techniques for future studies.

The Kona Dolomite contains evidence for complex diagenetic and metamorphic influence, which varies considerably over hand-sample scale. Because diagenetic effects, and particularly meteoric alteration, would tend to decrease $\delta^{13}C$ (if affected at all), we conservatively interpret samples with higher $\delta^{13}C$ (+6-8‰) as the closest to primary seawater values in the Kona region. It is plausible that more negative values resulted from secondary alteration, either during early cementation or greenschist metamorphism.

5.2.2. Facies variability

Despite evidence for alteration, a few patterns emerge when examining $\delta^{13}C$ between different Kona facies regardless of location (planar dolomite, domal and stratiform stromatolites) (Supp. Fig. S1). Of these facies, domal stromatolites contain the widest range of $\delta^{13}C$ values (+3.8 to + 7.9‰), similar to planar dolomite and stratiform stromatolites across the region. Two notable exceptions are domal samples LQ1-2 from Lindberg Quarry and MM3 from Mount Mesnard, which contain enriched $\delta^{13}C$ (~ +7.5‰) and depleted $\delta^{18}O$ (~ −13‰), the lightest $\delta^{18}O$ observed (Fig. 11, Table 1). Both LQ1-2 and MM3 are relatively fractured compared with other domal samples (Fig. 13), and as discussed in Section 5.3.1, we interpret their depleted $\delta^{18}O$ values as influenced by post-depositional meteoric fluids (Banner & Hanson, 1990; Swart, 2015) instead of primary facies variations. Otherwise, no distinctions can be made between domal stromatolites and other Kona facies (Supp. Fig. S1).

In contrast, stratiform stromatolites and planar dolomite have relatively different patterns of $\delta^{13}C$ and $\delta^{18}O$ (Supp. Fig. S1). Planar dolomites have lighter signatures ($\delta^{13}C$: ~ +5 to + 7‰; $\delta^{18}O$: ~ −13 to-10‰), while stratiform stromatolites typically have heavier signatures ($\delta^{13}C$: ~ +6 to + 8‰; $\delta^{18}O$: ~ −12 to −7‰), with one important exception. Many of the heaviest $\delta^{13}C$ values in this study (around + 8‰) come from SLQ1-1, a stratiform stromatolite with evaporite pseudomorphs (Fig. 10, Table 1, Supp. Figs. S1 and S2). Intriguingly, carbon isotopes in SLQ1-1 are bimodal, with a heavy cluster around + 8‰ and a much lighter cluster around + 5‰ (Supp. Fig. S1). Oxygen isotopes are similarly elevated across all SLQ1-1 samples (−10 to −7‰). The lighter $\delta^{13}C$ values around 5‰ form a notable outlier above with the majority of Kona samples, with depleted carbon but elevated oxygen isotopes (Fig. 11, Supp. Fig. S1).

Unlike the isotopic outliers in domal stromatolites (see previous paragraph), several lines of evidence argue against significant meteoric alteration causing this depleted $\delta^{13}C$ in SLQ1-1. Oxygen isotopes are more easily reset to depleted values in meteoric water (Banner & Hanson, 1990; Swart, 2015), and SLQ1-1 lacks the extensive fracturing of the domal samples (Supp. Fig. S2). Instead, the similarly enriched (and likely less altered) $\delta^{18}O$ across all SLQ1-1 samples favor primary or early diagenetic $\delta^{13}C$ fluctuations. One potential explanation for such distinct $\delta^{13}C$ patterns within a single evaporative stromatolite could be due to variable photosynthesis over time in very shallow microbial mats. Photosynthesis not only removes light $\delta^{13}C$ from local waters, but also increases carbonate saturation, precipitating carbonate minerals with heavier $\delta^{13}C$ than expected by 4‰ or higher (Geyman & Maloof, 2019). Such effects are amplified in shallower, poorly-mixed environments with high photosynthesis, such as evaporative tidal mats that formed SLQ1-1. In such a model, layers with heavier $\delta^{13}C$ (~ +8‰) could represent enhanced photosynthesis, while layers with lighter $\delta^{13}C$ (~ +5‰) could represent diminished photosynthesis or greater mixing with open-marine waters. While more samples are needed to test this hypothesis in the Kona Dolomite, the only evaporitic sample without stromatolites (480–1-1) has a much narrower $\delta^{13}C$ range (+5.8 to + 6.0‰) closer to lower values seen in stromatolitic SLQ1-1 (~ +5‰), as expected in a similar environment without photosynthetic mats.

5.2.3. Local and regional variability

The Kona Dolomite shifts from shallower, occasionally evaporitic supratidal and upper intertidal facies in the west to deeper intertidal and subtidal facies in the east. Despite these lateral trends, and differences between certain Kona facies (see 5.3.1), carbon isotopes remain indistinguishable between the shallower west and deeper east (Fig. 11). For example, western exposures such as Lindberg Quarry contain some of the most ^{13}C-enriched samples, but they are matched by samples in eastern Marquette both in our study and in Bekker et al., 2006 (Fig. 11). No stratigraphic trends across time were observed between west and east exposures (Fig. 11), though as previously mentioned, lateral correlation for many of Taylor 1972's informal members has not been verified across the basin.

There are several potential explanations for distinct facies with similar chemistry across the Kona Dolomite. First, it is possible that original $\delta^{13}C$ values of micritic carbonates did not vary significantly across the ~ 10 km study area, despite real differences in water depth and environment. Similar obscuring effects are observed in modern carbonate platforms such as the Bahamas. Geyman & Maloof (2021) compared $\delta^{13}C$ in Bahamian DIC and unconsolidated micrite, from the platform margin to coastal deposits ~ 50 km away. These distant locations had a 5‰ difference in local DIC, but micrite sediments in each location only had a 1‰ difference in $\delta^{13}C$ (Geyman & Maloof 2021). The study attributed similarities in micrite $\delta^{13}C$ to homogenization during transport of fine-grained muds. The Kona Dolomite samples from our study were collected over a much smaller transect, less than 10 km (Figs. 1, 2). Therefore, we interpret similar $\delta^{13}C$ values across distinct environments as influenced by the transport and mixture of carbonate mud across a shallow platform or ramp.

As discussed in 5.3.1, it is possible that secondary alteration has also homogenized or shifted isotope signals over time, either during early cementation or during metamorphosis. Future examination of isotopic values above and below unconformities in Lindberg Quarry could help test the possibility of early diagenesis. Another alternative is that the apparent facies differences between west and east Marquette could be an artifact of exposure availability. Many previous studies did not explicitly describe the lateral distribution of key facies indicators such as evaporite pseudomorphs or mud cracks, and extensive cover makes correlation increasingly difficult. Further investigation of obscured exposures will provide clearer connections between western and eastern Kona Dolomite, but our observations confirm previous evidence that facies become increasingly distal to the east (Taylor 1972; Wohlabaugh & Mancuso 1990).

One model explaining enriched $\delta^{13}C$ during the LJE invokes facies dependance: shallower, restricted evaporitic environments often have higher $\delta^{13}C$ than adjacent subtidal or open-marine deposits (Schidlowski et al., 1976; Melezhik et al.,1999; Frauenstein et al., 2009; Mayika et al., 2020; Prave et al., 2022). For example, during the LJE, $\delta^{13}C$ in intertidal-sabkha carbonates were ~ 8‰, nearshore-inner shelf carbonates were ~ 6.2‰, and open-deeper marine carbonates were only 1.5‰ (Prave et al., 2022, Hodgskiss et al., 2023). While eastern exposures lack evaporitic facies, their proximity within 10 km of the gypsum-bearing western deposits likely places them within the same restricted basin. If so, enhanced photosynthesis could have produced $\delta^{13}C$-enriched micrite within restricted waters as opposed to more open-marine settings, as observed in modern carbonate platforms (Geyman & Maloof, 2019; Chen et al., 2022; Trower et al., 2024). For example, Wohlabaugh 1980 describes the giant lakeshore stromatolites in the eastern Kona as being "oversteepened" to oncoming waves the east, potentially acting as an outer barrier for a "sheltered cove". If so, truly open-marine deposits with lower $\delta^{13}C$ could have been present to the east. Unfortunately, no known surface exposures exist beyond the lakeshore stromatolites in

Lake Superior (Figs. 1, 2).

While the Kona Dolomite by itself provides ambiguous evidence for a facies-dependent LJE, comparison with other regional LJE-era carbonates strongly supports the idea. Of the eight LJE-era carbonates in the Lake Superior region (Fig. 1), the only two members with reported evaporites (Kona, Gordon Lake) are also the only members with $\delta^{13}C$ over 5‰ (Taylor 1972; Cameron, 1983; Chandler, 1988; Wohlabaugh & Mancuso, 1990; Bekker et al., 2006). The isotopic similarities between $\delta^{13}C$ enriched Kona and Gordon Lake deposits were once interpreted as coeval deposition (Bekker et al., 2006), but this hypothesis has since been disproven by recent age dating (Kona = 2174 ± 9 Ma, Gordon Lake = 2318 ± 8 Ma, Rasmussen et al., 2024). The other LJE-era formations in the region (Bad River, Denham, Glen Township, Randville, Saunders, Trout Lake) average ~ 0‰, with a range of −3 to + 3‰ (Bekker et al., 2006). Detailed studies of these $\delta^{13}C$-"depleted" formations are rare, but no evaporites yet have been reported. Recent sedimentological study of the Randville Dolomite established a subtidal setting close to storm-weather wave base, with no evidence for evaporation (Brown et al., 2025). Therefore, the pattern of $\delta^{13}C$-enriched evaporitic carbonates and $\delta^{13}C$-"depleted" open-marine zones supports a facies-dependent LJE model in the Lake Superior region.

6. Conclusions

The Kona Dolomite is the most extensive LJE-era carbonate on the southern Superior Craton. In western exposures, evaporite pseudomorphs, roll-up structures and stratiform stromatolites were deposited in shallow tidal flats and sabkhas with pervasive microbial growth, subaerial exposure, and intermittent disturbances. A few km east, eastern facies include giant domal stromatolites and a lack of many features visible in the west, indicating a transition to somewhat deeper environments. Carbon isotopes across the Kona Dolomite demonstrate "classic" enriched LJE signatures (+4 to + 8‰), with no apparent variation due to facies changes. However, the evaporative Kona deposits are distinctly higher in $\delta^{13}C$ than surrounding carbonates with no evidence for similar restriction or evaporation. The contrast between $\delta^{13}C$-enriched, evaporitic carbonates such as the Kona and depleted, open-marine neighbors supports previous hypotheses of broad facies-dependent drivers during the LJE.

CRediT authorship contribution statement

Maya L. Giannecchini: Investigation, Funding acquisition, Formal analysis, Data curation, Conceptualization. **Garrett D. Brown:** Funding acquisition, Formal analysis, Data curation. **Cory M. Redman:** Writing – review & editing, Validation, Investigation, Data curation. **Ian Z. Winkelstern:** Writing – review & editing, Validation. **Dylan T. Wilmeth:** Writing – review & editing, Supervision, Methodology, Investigation, Data curation, Conceptualization.

Declaration of competing interest

The authors declare that they have no known competing financial interests or personal relationships that could have appeared to influence the work reported in this paper.

Appendix A. Supplementary data

Supplementary data to this article can be found online at https://doi.org/10.1016/j.precamres.2026.108107.

Data availability

Data will be made available on request.

References

Aharon, P., Kolodny, Y., Sass, E., 1977. Recent hot brine dolomitization in the" solar lake," gulf of elat, isotopic, chemical, and mineralogical study. J. Geol. 85, 27–48.

Altermann, W., 2008. Accretion, trapping and binding of sediment in archean stromatolites—morphological expression of the antiquity of life. Space Sci. Rev. 135, 55–79. https://doi.org/10.1007/s11214-007-9292-1.

Banner, J.L., Hanson, G.N., 1990. Calculation of simultaneous isotopic and trace element variations during water-rock interaction with applications to carbonate diagenesis. Geochim. Cosmochim. Acta 54, 3123–3137.

Bekker, A., Karhu, J.A., Kaufman, A.J., 2006. Carbon isotope record for the onset of the Lomagundi carbon isotope excursion in the Great Lakes area, North America. Precambr. Res. 148, 145–180. https://doi.org/10.1016/j.precamres.2006.03.008.

Bindeman, I.N., 2021. Triple oxygen isotopes in evolving continental crust, granites, and clastic sediments. Rev. Mineral. Geochem. 86, 241–290. https://doi.org/10.2138/rmg.2021.86.08.

Cameron, E.M., 1983. Evidence from early Proterozoic anhydrite for sulphur isotopic partitioning in Precambrian oceans. Nature 304, 54–56. https://doi.org/10.1038/304054a0.

Cannon, W.F., Gair, J.E., 1970. A revision of stratigraphic nomenclature of middle Precambrian rocks in northern Michigan. Geol. Soc. Am Bull 81.

Chandler, F.W., 1988. Diagenesis of sabkha-related, sulphate nodules in the early Proterozoic Gordon Lake formation, Ontario, Canada. Carbonates Evaporites 3, 75–94. https://doi.org/10.1007/BF03174414.

Chen, M., Conroy, J.L., Geyman, E.C., Sanford, R.A., Chee-Sanford, J.C., Connor, L.M., 2022. Stable carbon isotope values of syndepositional carbonate spherules and micrite record spatial and temporal changes in photosynthesis intensity. Geobiology 20, 667–689.

Frauenstein, F., Veizer, J., Beukes, N., Van Niekerk, H.S., Coetzee, L.L., 2009. Transvaal supergroup carbonates: implications for paleoproterozoic δ18O and δ13C records. Precambr. Res. 175, 149–160. https://doi.org/10.1016/j.precamres.2009.09.005.

Gair, J., TM, H., 1975. Bedrock Geology And Ore Deposits Of The Palmer Quadrangle, Marquette County, Michigan. Bedrock Geology And Ore Deposits Of The Palmer Quadrangle, Marquette County, Michigan.

Gair, J.E., Thaden, R.E., 1968. Geology of the Marquette and Sands quadrangles, Marquette County, Michigan. Professional Paper. Doi: 10.3133/pp397.

Geyman, E.C., Maloof, A.C., 2019. A diurnal carbon engine explains 13C-enriched carbonates without increasing the global production of oxygen. Proc. Natl. Acad. Sci. 116, 24433–24439.

Geyman, E.C., Maloof, A.C., 2021. Facies control on carbonate δ13C on the Great Bahama Bank. Geology 49, 1049–1054.

Grey, K., Awramik, S., 2020. Handbook for the study and description of microbialites. Geological Survey of Western Australia Bulletin 147.

Hagadorn, J.W., Mcdowell, C., 2012. Microbial influence on erosion, grain transport and bedform genesis in sandy substrates under unidirectional flow. Sedimentology 59, 795–808.

Hodgskiss, M.S.W., Crockford, P.W., Turchyn, A.V., 2023. Deconstructing the lomagundi-jatuli carbon isotope excursion. Annu. Rev. Earth Planet. Sci. 51, 301–330. https://doi.org/10.1146/annurev-earth-031621-071250.

James, H.L., 1955. Zones of regional metamorphism in the precambrian of Northern Michigan. GSA Bull. 66, 1455–1488. https://doi.org/10.1130/0016-7606(1955)66[1455:ZORMIT]2.0.CO;2.

James, H.L., Clark, L.D., Lamey, C.A., Pettijohn, F.J., 1961. Geology of central Dickinson County, Michigan. Professional Paper. Doi: 10.3133/pp310.

Kah, L.C., Knoll, A.H., 1996. Microbenthic distribution of Proterozoic tidal flats: environmental and taphonomic considerations. Geology 24, 79–82. https://doi.org/10.1130/0091-7613(1996)024<0079:MDOPTF>2.3.CO;2.

Karhu, J.A., Holland, H.D., 1996. Carbon isotopes and the rise of atmospheric oxygen. Geology 24, 867–870. https://doi.org/10.1130/0091-7613(1996)024<0867:CIATRO>2.3.CO;2.

Kaufman, A.J., Jacobsen, S.B., Knoll, A.H., 1993. The Vendian record of Sr and C isotopic variations in seawater: implications for tectonics and paleoclimate. Earth Planet. Sci. Lett. 120, 409–430. https://doi.org/10.1016/0012-821X(93)90254-7.

Kaufman, A.J., Knoll, A.H., 1995. Neoproterozoic variations in the C-isotopic composition of seawater: stratigraphic and biogeochemical implications. Precambr. Res. 73, 27–49. https://doi.org/10.1016/0301-9268(94)00070-8.

Larue, D.K., 1981. The chocolay group, lake superior region, U.S.A.: sedimentologic evidence for deposition in basinal and platform settings on an early Proterozoic craton. GSA Bull. 92, 417–435. https://doi.org/10.1130/0016-7606(1981)92<417:TCGLSR>2.0.CO;2.

Logan, B.W., 1961. Cryptozoon and associate stromatolites from the recent, Shark Bay, Western Australia. J. Geol. 69, 517–533.

Martin, A.P., Condon, D.J., Prave, A.R., Lepland, A., 2013. A review of temporal constraints for the Palaeoproterozoic large, positive carbonate carbon isotope excursion (the Lomagundi–Jatuli Event). Earth Sci. Rev. 127, 242–261. https://doi.org/10.1016/j.earscirev.2013.10.006.

Mayika, K.B., Moussavou, M., Prave, A.R., Lepland, A., Mbina, M., Kirsimäe, K., 2020. The paleoproterozoic francevillian succession of gabon and the lomagundi-jatuli event. Geology 48, 1099–1104. https://doi.org/10.1130/G47651.1.

Melezhik, V.A., Fallick, A.E., Medvedev, P.V., Makarikhin, V.V., 1999. Ga magnesite–stromatolite–dolomite–'red beds' association in a global context: a case for the world-wide signal enhanced by a local environment.

Pettijohn, F.J., 1943. Basal huronian conglomerates of menominee and Calumet Districts, Michigan. J. Geol. 51, 387–397. https://doi.org/10.1086/625162.

Prave, A.R., Kirsimäe, K., Lepland, A., Fallick, A.E., Kreitsmann, T., Deines, Y.E., Romashkin, A.E., Rychanchik, D.V., Medvedev, P.V., Moussavou, M., Bakakas, K.,

Hodgskiss, M.S.W., 2022. The grandest of them all: the Lomagundi–Jatuli Event and Earth's oxygenation. JGS 179, jgs2021-036. https://doi.org/10.1144/jgs2021-036.
Puffett, W.P., 1974. Geology of the Negaunee quadrangle, Marquette County, Michigan (No. 788), Professional Paper. U.S. Government Printing Office. Doi: 10.3133/pp788.
Ramsay, B., Fralick, P., Homann, M., Lalonde, S., Riding, R., 2025. Early Paleoproterozoic warming and oxidation of the Planet recorded by sedimentology and rare earth elements of two Huronian carbonate deposits. Precambr. Res. 427, 107886.
Rasmussen, B., Zi, J., Bekker, A., 2024. New U-Pb zircon tuff ages and revised stratigraphic correlations in the Superior craton during the Great Oxidation Episode. Earth Planet. Sci. Lett. 640, 118779. https://doi.org/10.1016/j.epsl.2024.118779.
Schidlowski, M., Eichmann, R., Junge, C.E., 1976. Carbon isotope geochemistry of the Precambrian Lomagundi carbonate province, Rhodesia. Geochim. Cosmochim. Acta 40, 449–455. https://doi.org/10.1016/0016-7037(76)90010-7.
Schidlowski, M., 1985. Carbon isotope discrepancy between Precambrian stromatolites and their modern analogs: inferences from hypersaline microbial mats of the Sinai coast. Orig. Life Evol. Biosph. 15, 263–277.
Shapiro, R., Wilmeth, D., 2020. Treatise Online no. 134: Part B, Volume 2, Chapter 8: Microbialites. Treatise Online. Doi: 10.17161/to.vi.13862.
Swart, P.K., Reijmer, J.J., Otto, R., 2009. A re-evaluation of facies on great Bahama bank II: Variations in the δ13C, δ18O and mineralogy of surface sediments. Perspectives in carbonate geology: A tribute to the career of Robert Nathan Ginsburg 47–59.
Swart, P.K., 2015. The geochemistry of carbonate diagenesis: the past, present and future. Sedimentology 62, 1233–1304.
Taylor, L., 1972. Stratigraphy, sedimentology, and sulfide mineralization of the Kona Dolomite (Ph.D.). Michigan Technological Institute, Lansing, Michigan.
Tilley, C.E., 1948. Earlier stages in the metamorphism of siliceous dolomites (with Plates XVII and XVIII.). Mineral. Mag. J. Mineral. Soc. 28, 272–276. https://doi.org/10.1180/minmag.1948.028.200.03.
Tostevin, R., Shields, G.A., Tarbuck, G.M., He, T., Clarkson, M.O., Wood, R.A., 2016. Effective use of cerium anomalies as a redox proxy in carbonate-dominated marine settings. Chem. Geol. 438, 146–162.
Trower, E.J., Hibner, B.M., Lincoln, T.A., Dodd, J.E., Hagen, C.J., Cantine, M.D., Gomes, M.L., 2024. Revisiting elevated δ13C values of sediment on modern carbonate platforms. Geophys. Res. Lett. 51.
Twenhofel, W.H., 1919. Pre-Cambrian and carboniferous algal deposits. Am. J. Sci. 4, 339–352.
Vallini, D.A., Cannon, W.F., Schulz, K.J., 2006. Age constraints for Paleoproterozoic glaciation in the Lake Superior Region: detrital zircon and hydrothermal xenotime ages for the Chocolay Group, Marquette Range Supergroup. Can. J. Earth Sci. 43, 571–591. https://doi.org/10.1139/e06-010.
Veizer, J., 1983, Chemical Diagenesis of Carbonates: Theory and Application of Trace Element Technique, *in* Arthur, M.A., Anderson, T.F., Kaplan, I.R., Veizer, J., and Land, L.S. eds., Stable Isotopes in Sedimentary Geology, SEPM Society for Sedimentary Geology, v. 10, p. 0, doi:10.2110/scn.83.01.0000.
Wohlabaugh, N., 1980. Petrology of the Big Cusp Algal Dolomite; An informal member of the Kona Dolomite, Marquette, Michigan (M.Sc. Thesis). Bowling Green State University, Ohio.
Wohlabaugh, N., Mancuso, J.J., 1990. Depositional and diagenetic history of the big Cusp Algal Dolomite, Kona Formation, Marquette Range, Michigan. The Compass 67, 84–93.